ATOMIC BEAM STUDIES OF INDIUM 117m

ATOMIC BEAM STUDIES OF INDIUM 117m

By

ATIQUE-UR-RAHMAN MUFTI

A Thesis

Submitted to the Faculty of Graduate Studies

in Partial Fulfilment of the Requirements

for the Degree

Master of Science

McMaster University

September, 1966

MASTER OF SCIENCE (1966) McMASTER UNIVERSITY
(Physics) Hamilton, Ontario

TITLE: Atomic Beam Studies of In^{117m}

AUTHOR: Atique-Ur-Rahman Mufti, M.Sc. (Panjab)

SUPERVISOR: Dr. R. G. Summers-Gill

NUMBER OF PAGES: viii, 63

SCOPE AND CONTENTS:

The atomic beam magnetic resonance technique with radioactive detection has been used to investigate the hyperfine structure of In^{117m}. The present research is based on the work done by Cameron (1962) who could not obtain accurate values for the hyperfine interaction constants due to the low neutron flux at the time in the McMaster reactor.

This thesis is an account of an attempt to complete that experiment by observing the field independent direct hyperfine transitions. The theory of the experiment, the apparatus and techniques, and the method of data analysis are described. Because of the counting errors, the data are not as conclusive as had been hoped. If the resonances have, in fact, been seen, then the results are:

$$a_{1/2} = -932.996 \pm 0.012 \text{ Mc/sec}$$

$$a_{3/2} = -99.005 \pm 0.005 \text{ Mc/sec}$$

$$\mu_I = -0.25146 \pm 0.00003 \text{ nuclear magnetons.}$$

ACKNOWLEDGEMENTS

I must express my most sincere thanks to the External Aid Office, Ottawa, for the financial aid and for my maintenance in Canada in a respectable way, Pakistan Atomic Energy Commission for sponsering my training abroad and the National Research Council for the grants to the Physics Department.

I must also thank Dr. R. G. Summers-Gill and Dr. J. A. Cameron for their help and guidance for this research problem.

I think I shall be leaving a big formality if I do not mention the names of my colleagues, Messrs. A. R. Pierce, J. H. Robertson, G. M. Stinsen, J. Murrey and T. McMath, for their interest. I am particularly grateful to my colleague Mr. J. C. Waddington, without whose good and accommodating nature I could not have continued with my research project.

Mr. J. B. McDougall and the Reactor Staff deserve my most sincere thanks.

I would like to express my thanks to my friend Mr. H. B. Bayley about whom I can say that a friend in need is a friend indeed.

It will be inappropriate if I do not express my thanks to some of my colleagues who have voluntarily been acting as a one sided communicator, because their efforts contributed a lot in my life and personality at the McMaster University.

If at all I am permitted to add one more acknowledgement then certainly I would like to admit my sincere thanks to the first aid box on the receptionist's desk from which I had to get quite often the asprin tablets, and to the doctor who advised me for my abnormally fast turning grey hair.

I dedicate this research work to my rational and patriotic spirit which survived inspite of all the difficulties.

TABLE OF CONTENTS

LIST OF FIGURES

CHAPTER I

INTRODUCTION

The history of atomic beams, a little more than half a century old, can be traced back to 1911 when Dunoyer (1911) studied the trajectories of sodium atoms in an evacuated tube. Stern and Gerlach (1921) introduced a new concept to the old experiments when they proved space quantization. Precise measurements of atomic and nuclear properties were initiated by Rabi and associates (1938) with the introduction of the resonance method. Since that time the popularity and scope of atomic beam measurements have been influenced mainly by various technical advances in r.f. equipment and detection methods.

Experiments have been performed to measure such diverse atomic and nuclear properties as electronic and nuclear angular momenta and gyromagnetic ratios, hyperfine interaction constants, isotope shifts, hyperfine anomalies, etc. Nor have the measurements been confined to atomic ground states or stable isotopes. In some instances the quantities determined are the most precisely known physical constants.

Construction of the atomic beam machine at McMaster University was started in 1957 and the first experiment - the determination of the spin of indium - 115m - was completed in 1960 (King, 1960 and King et al., 1961). Since then a number of radioactive elements such as Ag^{109m}, Cs^{138}, In^{115m}, In^{117}, In^{117m}, Sm^{153} and Sm^{155} have been studied.

Cameron (1962) measured the values of a ($^2P_{3/2}$) and a ($^2P_{1/2}$) for In^{115m} and from them deduced μ_I but he could not succeed in finding similarly precise values for In^{117m}. The biggest handicap to his experiment on In^{117m} was that he could not produce strong enough sources due to the low neutron flux in the reactor. However, he did determine that the nuclear spin is ½ (Cameron et al. 1962) and, on the basis of measurements of the $\Delta F = 0$ transition in the $^2P_{1/2}$ state at high field (~500 gauss), concluded the following:

$$a(^2P_{1/2}) = (-)\ 931.5 \pm 2.0 \text{ Mc/sec}$$

$$\mu_I = (-)\ 0.2510 \pm 0.0005 \text{ nuclear magneton.}$$

Since that time, the neutron flux of the McMaster reactor has been raised considerably (though not as much as had been hoped). Accordingly it was thought to be worthwhile to give the In^{117m} experiment a further try.

Before starting with the theory of the atomic beam experiment (Chapter II) it seems appropriate to give a little introduction to nuclear moments and models.

A nucleus interacts with an external electromagnetic system such as the atomic electron through its electromagnetic properties - charge density and current density. It is convenient to express these interactions in terms of multipoles. Thus the interaction energy is represented by a sum of terms proportional to nuclear moments, i.e. monopole, dipole, quadrupole, etc. Because the electrons are far from the nucleus, relative to its dimensions, the terms in the series diminish rapidly in importance. Only in a few cases has even the octupole energy been detected.

The electric and magnetic multipole operators of order λ are written as:

$$Q_\lambda^\mu = e \sum_{k=1}^{Z} r_k^\lambda \; Y_\lambda^\mu (\theta_k) \qquad \text{(I-1)}$$

$$M_\lambda^\mu = \mu_N \sum_{k=1}^{A} \nabla (r_k^\lambda \; Y_\lambda^\mu (\theta_k)) \cdot \left[g_\ell \; \frac{2\vec{\ell}_k}{\lambda+1} + g_S \; \vec{S}_k \right]$$

Where e is electronic charge and μ_N is nuclear magneton. The co-ordinates of the kth nucleon are denoted by r_k, θ_k and ϕ_k, g_s and g_ℓ are the spin and orbital gyromagnetic ratios having values

$g_s = -3.826$, $g_\ell = 0$ for neutrons and $g_s = 5.586$, $g_\ell = 1$ for protons, and $Y^{\mu}_{\lambda}(\theta_k)$ is a spherical tensor of order λ and projection μ.

From the classical point of view the multipole expansion contains an infinite number of terms, but quantum mechanical considerations limit the expansion. Only for $k \leqslant 2I$ can a nucleus with spin I have non-zero static 2^k-pole moments. In addition, the expectation value of an odd parity operator is zero. Since the parity of Q^{μ}_{λ} is $(-1)^{\lambda}$ and that of M^{μ}_{λ} is $(-1)^{\lambda+1}$, the observable static moments are limited to electric monopole, quadrupole, etc., and magnetic dipole, octupole, etc.

As Equation (I-1) is impossibly difficult to evaluate, except in the case of simple nuclei, some simplifying assumptions have to be made in order to treat complex nuclei. On the basis of these a few nuclear models, such as nuclear shell model and collective model have been introduced and successfully applied in different mass regions.

The shell model is based on a number of assumptions. Each nucleon moves in a static central potential, which represents the average interaction of the nucleon with the remaining nucleons of the nucleus. The potential is quite different from the Coulomb potential. It has a form between the square well potential $V = -V_o$ and the so-called oscillator potential $V = -V_o + ar^2$ where r is the distance between the nucleon and the centre of force and a is a constant. It is also necessary to introduce a strong spin-orbit

coupling. The nucleons will then arrange themselves in different energy levels according to the Pauli exclusion principle. When a shell is filled the resulting configuration is particularly stable, thus explaining the observed magic numbers.

A further assumption in the extreme single particle model is that not only filled nucleon shells, but also even numbers of neutrons, or protons in any level have no net angular momentum and no magnetic moments. In a nucleus of odd A, all but one of the nucleons are considered to have their angular momenta paired off, forming an even-even "core"; the single odd nucleon is thought to move essentially independently in (or outside) this core, and the net angular momentum of the entire nucleus is determined by the quantum state of this nucleon. The moments of odd-mass nuclei are assumed to arise from the single unpaired nucleon, and this reasoning leads, for example, to the Schmidt values for magnetic dipole moments.

Although the shell model is quite successful in predicting the ground state spins and parities, and isomeric states of odd A nuclei the theoretical values of magnetic dipole and electric quadrupole moments are not in as close harmony with experiment. This discrepancy is attributed to the inadequate account of inter-nucleon forces in the simple model.

In a more realistic shell model only the nucleons in completely filled major shells are assumed to couple to spin zero. Outside this core, the nucleons move subject to a particle spin-orbit interaction, a mean particle-core interaction, and a residual particle-particle interaction. The latter is assumed to be small compared to the effective single particle force and is treated as a perturbation. Single particle wave functions are used as a basis of "configuration mixing" calculations.

The shell model does not predict the very large electric quadrupole moments observed in certain nuclei. This failure, together with the observation of systematically spaced energy levels in neighbouring even-even nuclei, suggested a quite different approach. This collective model was initially developed by Bohr and then generalized and extended by him and Mottelson (Bohr and Mottelson, 1953), by Nilsson (1955) and since then by many others. Far from the closed shells of the shell model the effect of the "loose" nucleons can be quite large making it possible for the core to take up a non-spherical shape. Thus collective surface oscillations are possible. In the rare earths and actinides, where the large quadrupole moments appear, it is clear that it becomes energetically favourable for the nucleus to retain a permanent deformation. Collective rotations then occur and the energies and decay modes of these low-lying states provide a sensitive measure of the degree of

deformation. This can be used to calculate electric quadrupole moments which are found to be in substantial agreement with those observed. In the model the core shares in the angular momentum so calculated magnetic dipole moments differ from those of the shell model.

CHAPTER II

THEORY OF THE EXPERIMENT

1 - Hyperfine Interaction in a Free Atom

The atomic beam resonance method is based on the interaction of the nucleus and electrons with each other and with externally applied magnetic fields. The total atomic Hamiltonian, in the absence of an external magnetic field may be written as

$$H_{total} = H_{nuclear} + H_{electronic} + H_{hyperfine} .$$

The first term on the right hand side represents the internal energy of the nucleus. In view of the widely spaced nuclear energy levels, of the order of tens or hundreds of kilo electrons volts, as compared to electronic energy levels separated by 1 e.v., the nucleus is usually considered to be in a single eigenstate, which is characterised by nuclear spin denoted by I. Hence, the $H_{nuclear}$ term may be ignored in further detailed treatment. The second term, $H_{electronic}$, is responsible for gross and fine structure of atomic optical spectrum. It describes the interaction of the electrons with the nucleus in the assumption that the latter

is a point charge. It also includes the interaction of the electrons with one another. In atoms where the fine structure states are well separated ($\gtrsim$ 1000 cm^{-1}) it is usually sufficient to treat this term in much the same way as above. That is, the electrons may be regarded as being in a specified state of $H_{electronic}$ with angular momentum J.

The last term gives rise to hyperfine structure splitting of the electronic levels. Since 1924, when Pauli postulated that hyperfine structure could be attributed to the interaction between the nuclear and electronic angular momenta, a number of different theoretical treatments have been put forward to calculate it (Goudsmit, 1931, Breit and Wills, 1933, Schwartz, 1955).

As mentioned in Chapter I, the hyperfine interaction consists of a series of terms in which the 2^{λ} -pole of the nucleus interacts with the 2^{λ} pole component of the electronic field. So $H_{hyperfine}$ is the sum of a number of expressions, such as the magnetic dipole interaction given by

$$H_{MI} = ha\ \vec{I}.\vec{J},$$

the electric quadrupole interaction

$$H_{E2} = ha\ \frac{3(\vec{I}.\vec{J})^2 + \frac{3}{2}(\vec{I}.\vec{J}) - I(I+1)\,J(J+1)}{2I(2I-1)\,J(2J-1)},$$

and the magnetic octupole interaction

$$H_{M3} = hc \frac{10(\vec{I}\cdot\vec{J})^3+20(\vec{I}\cdot\vec{J})^2+2(\vec{I}\cdot\vec{J})\left[-3I(I+1)J(J+1)+I(I+1)+J(J+1)+3\right]-5I(I+1)J(J+1)}{I(I-1)\ (2I-1)\ J(J-1)\ (2J-1)}$$

The quantities a, b and c are constants having the units of frequency related to the nuclear moments as shown below:

$$a = \frac{\mu_I}{I} \quad \text{x electronic factor}$$

$$b = Q \text{ x electronic factor}$$

$$c = \Omega \text{ x electronic factor.}$$

Other higher order multipole interactions are negligible to the present limit of experimental accuracy.

If we take $\vec{F} = \vec{I} + \vec{J}$ as the total angular momentum of the atom, then

$$\vec{I}\cdot\vec{J} = \tfrac{1}{2}\left[F(F+1) - I(I+1) - J(J+1)\right]$$

The hyperfine energy of a state of given I, J and F is easily obtained by substituting this into the above expressions.

As a result of the relationship between a and μ_I, a simple equation holds for isotopes in the same electronic state. Referred to as the Fermi-Segrè formula, this is

$$\frac{a_1}{a_2} = \left(\frac{\mu_I}{I}\right)_1 \Big/ \left(\frac{\mu_I}{I}\right)_2 .$$

Small departures called hyperfine anomalies occur, particularly in $^2S_{1/2}$ atoms, because of the finite size of the nucleus.

2 - Hyperfine Interaction in the Presence of External Magnetic Field

In the presence of an external magnetic field another term representing interaction of the electronic and nuclear magnetic moments with the field must be added to the hyperfine Hamiltonian. Therefore,

$$H_{total} = H_{hyperfine} + H_{mag}$$

where

$$H_{mag} = - \vec{\mu}_J \cdot \vec{H} - \vec{\mu}_I \cdot \vec{H}$$

$\vec{\mu}_I = g_I \vec{I} \mu_o$ is the nuclear magnetic moment.

$\vec{\mu}_J = g_J \vec{J} \mu_o$ is the electronic magnetic moment.

and $\mu_o = \frac{eh}{2mc}$ is the Bohr magneton.

If the magnetic field is assumed to be in the Z direction then

$$H_{Mag} = - g_I I_z \mu_o H - g_J \mu_o J_z H.$$

It should be noted here that g_I is much smaller in magnitude than g_J. In nuclear physics g_I is of the order of unity since the nuclear magnetic moment is expressed in nuclear not Bohr magnetons.

As pointed out in the previous section $H_{hyperine}$ is diagonal in an (F,m) representation, but after the magnetic field is applied the spherical symmetry is lost and F is no longer a good quantum number. Its Z-component is, however, so the (F,m) representation is a convenient one for diagonalizing the Hamiltonian. Since $F_z = I_z + J_z$, it follows that

$$\langle F,m \mid I_z \mid F',m' \rangle = m \delta_{FF'} \delta_{mm'} - \langle F,m \mid J_z \mid F',m' \rangle$$

where $\delta_{FF'}$ and $\delta_{mm'}$ are Kronecker deltas.

The only non-zero matrix elements of J_z are

$$\langle F,m \mid J_z \mid F,m \rangle = \frac{F(F+1) + J(J+1) - I(I+1)m}{2F(F+1)}$$

$$\langle F,m \mid J_z \mid F-1, m \rangle = \langle F-1, m \mid J_z \mid F,m \rangle$$

$$= \frac{\left[(F-I+J)\,(F+I-J)\,(I+J+1+F)\,(I+J+1-F)\,(F^2-m^2) \right]^{1/2}}{4\,F^2(2F+1)\,(2F-1)}$$

By applying these expressions the Hamiltonian matrix can be divided into $2(I + J) + 1$ submatrices along the diagonal. Each submatrix corresponds to a different value of m, and the order of each submatrix is equal to the number of different F values contributing to it. Hence, we find that the secular equation is reduced to 2J+2I+1 factors. These are equated to zero to obtain the eigenvalues.

In case of $J = \frac{1}{2}$ the highest order determinants are 2 x 2 and can be solved easily. Following Breit and Rabi, the eigenvalues are usually written

$$W(F = I \pm \tfrac{1}{2}, m) = -\frac{ha}{4} - \frac{\mu_I}{I} Hm \pm \frac{ha}{4}(2I+1)\left[1 + \frac{4m}{2I+1}x + x^2\right]^{\frac{1}{2}}$$

where $x = -\dfrac{2(2\mu_J - \frac{\mu_I}{I})}{ha(2I = 1)} H$

For the case of $I = \frac{1}{2}$, which is appropriate for In^{117m}, the solution for arbitrary values of J can be written as

$$W(F=J\pm\tfrac{1}{2}m) = -\frac{ha}{4} - \frac{\mu_J}{J} H m \pm \frac{ha}{4}(2J+1)\left[1 + \frac{4m}{2J+1} y + y^2\right]^{\frac{1}{2}}$$

where $y = -2\dfrac{\left(\frac{\mu_I}{I} - \frac{\mu_J}{J}\right)}{ha(2J+1)} H.$

For the sake of interest Figure 1 shows the solution for the cases $I = \frac{1}{2}$, $J = \frac{1}{2}$ and $3/2$ assuming μ_I and "a" to be negative.

For the case of I and J both greater than $\frac{1}{2}$ the exact solution of secular equation presents some difficulties. An alternative method, the application of perturbation theory is useful.

FIGURE 1 ZEEMAN SPLITTING

Energy level diagram for (a) $J = \frac{1}{2}$, $I = \frac{1}{2}$, $\mu_I < 0$ and (b) $J = 3/2$, $I = \frac{1}{2}$, $\mu_I < 0$. Transitions of the type $\Delta F = 0$, which may be focussed in the "flop-in" configuration, are indicated by the double-ended arrows.

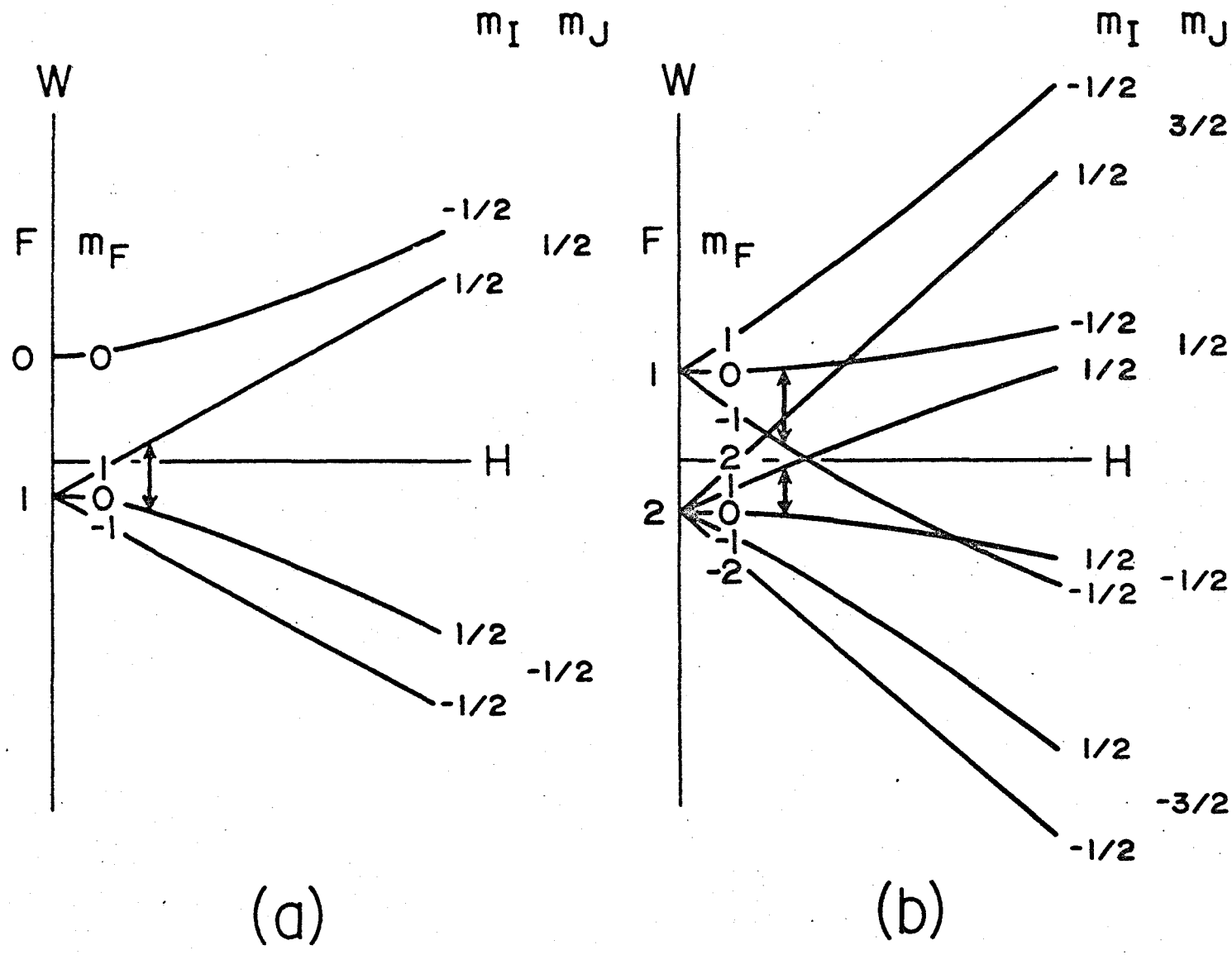
m_I m_J
W
F m_F
0
0
1
1
0
-1
H
-1/2
1/2
1/2
-1/2
(a)
m_I m_J
W
F m_F
1
0
-1
2
1
0
-1
-2
H
-1/2
3/2
1/2
-1/2
1/2
1/2
-1/2
1/2
-3/2
-1/2
(b)

3 - Deflection and Focussing of Atomic Beam

In an atomic beam machine the atoms pass in succession through an inhomogeneous magnetic field A, a homogeneous magnetic field C and a further inhomogeneous magnetic field B. While travelling through the regions of inhomogeneous magnetic field they experience deflecting forces

$$\vec{F} = - \nabla W = - \frac{\partial W}{\partial H} \nabla H = \mu_{eff} \nabla H.$$

Ramsey (1956) has shown that, independent of speed, the condition for refocussing the atoms on a detector placed on the axis of the machine is

$$\frac{H_A}{H_B} = K \left[\frac{(\mu_{eff})_B}{(\mu_{eff})_A} \right] .$$

The sign of μ_{eff} depends upon the quantum state of the atom and the magnitude of the field. The constant K, which depends upon the dimensions of the machine, can be negative or positive depending upon the relative directions of the field gradients.

In the homogeneous magnetic field region a weak radio-frequency oscillating field induces transitions between the magnetic substates of the atom. In a flop-in type machine (used for the present research), the value of K is negative, and only those atoms

can reach the detector which undergo transitions between states whose effective moments have opposite sign. Hence, at resonance, the beam intensity increases unlike the flop-out arrangement where, on a constant background, signal a decrease in beam intensity occurs.

4 - Atomic Beam Resonances

As the transitions to be induced involve states of the same parity, the selection rules are those of magnetic dipole radiation:

$$\Delta F = 0, \pm 1 \qquad \Delta m = 0, \pm 1 .$$

The σ transitions are those in which m does not change and are produced when the oscillating field is parallel to that of the static field direction. In π transitions m changes and they are induced by an oscillating field whose direction is perpendicular to the static field. In the case of sufficiently large r.f. magnetic field transitions can be induced which violate the above selection rules. The theory of these transitions, commonly known as multiple quantum transitions, have been investigated by several workers. (Hack, 1956,). They are not of concern in this problem.

When these conditions are combined with the requirement for observability one can readily determine the transitions which may be investigated. Their frequencies are given by the Bohr condition

$$W_{Fm} - W_{F'm'} = h \nu_o$$

where the energies of the upper and lower states, W_{Fm} and $W_{F'm'}$ respectively, are given by the solution of the Hamiltonian.

In Figure 1, the arrows indicate the observable $\Delta F = 0$ transitions. Their frequencies increase linearly from zero at zero field, when the magnetic substates are degenerate, through the linear Zeeman region. At higher fields, quadratic and higher order terms become important, but exact expressions are readily obtained from the Breit-Rabi equation.

For $F = \pm 1$, a number of σ- and π-transitions are usually observable. The most useful are those whose frequencies are independent of field to first order at some value of the field. In the cases of $I = \frac{1}{2}$, $J = \frac{1}{2}$ and $3/2$, appropriate to indium - 115 m and indium -117 m, the transitions $m_F = 0 \leftrightarrow m_F = 0$ are "field independent" at zero field. To order H^2 these σ transitions have frequencies given by

$$\nu_{1/2} = |a_{1/2}| \quad (1+x^2)^{1/2} \approx |a_{1/2}| + \frac{2(\mu_J - \mu_I)^2}{|a_{1/2}|} \quad \frac{H^2}{h^2}$$

and

$$\nu_{3/2} = 2|a_{3/2}| \quad (1+y^2)^{1/2} \approx 2|a_{3/2}| + \frac{(\mu_{J/3} - \mu_I)^2}{|a_{3/2}|} \quad \frac{H^2}{h^2} .$$

One might think that changes in the detected beam intensity would occur only when the transition frequency is applied. This is not the case for two reasons. Because the atom spends only

a short time τ in the transition region, the uncertainty principle dictates that a resonance will be broadened by an amount of the order of $\frac{1}{\tau}$ cycles/second. In addition, because the magnetic field in the transition region is not perfectly homogeneous the resonance line-width is even greater. The virtue of the field independent transition is the fact that this second contribution is minimized.

The slope of the resonance is also a concern. Provided that the r.f. power is not too great, a π-transition exhibits a bell-shaped curve centred on the transition frequency and with a full width at half maximum of typically 100 kilocycles per second. The antenna used in this work to induce σ -transitions produces a magnetic field that reverses direction at its centre. Consequently, the σ -resonances have a double hump with the valley between occurring at the true transition frequency (Cameron, 1962). These shapes are shown schematically in Figure 2.

FIGURE 2 RESONANCE SHAPES

A schematic diagram of the resonance curve shapes. The diagrams are drawn without any scale just to indicate the shape of (a) π resonance; (b) σ resonance. P stands for the transition probability at a given frequency. For details (Cameron (1962)).

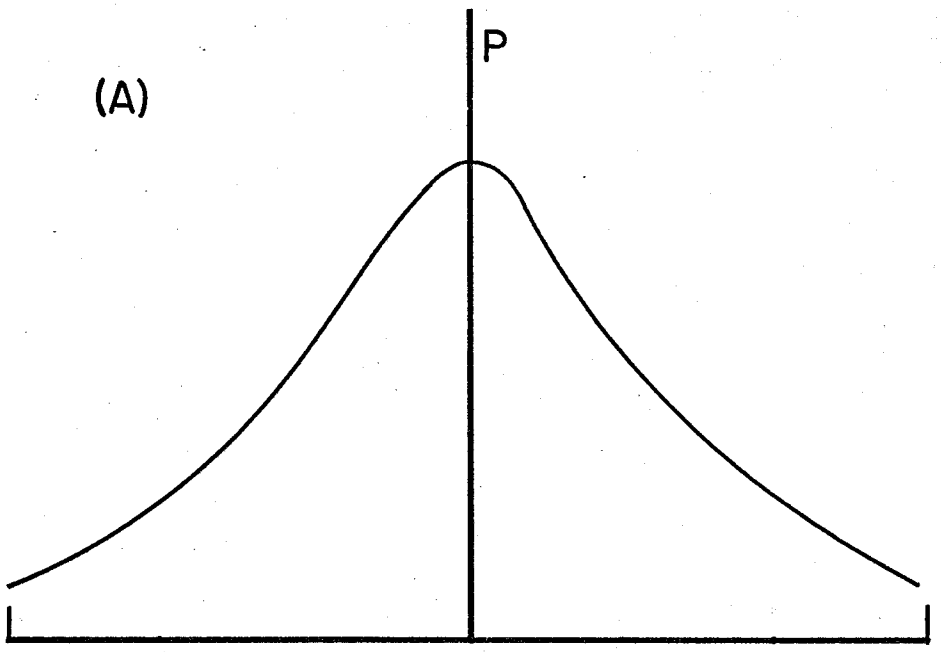
(A)
P
FREQUENCY

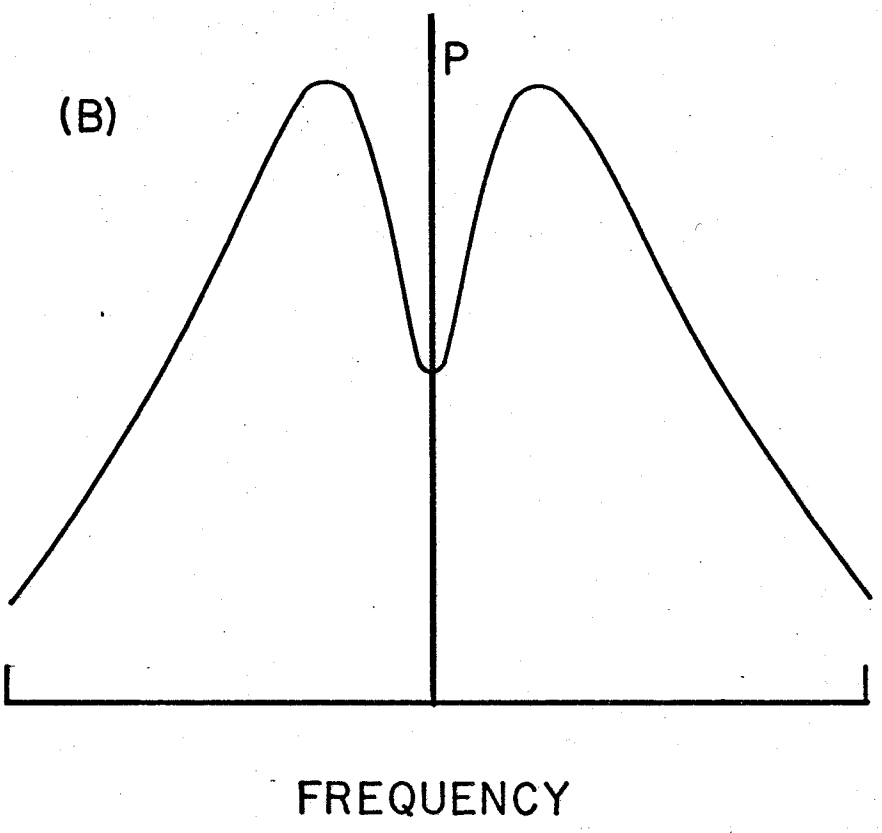
(B)
P
FREQUENCY

CHAPTER III

THE ATOMIC BEAM APPARATUS

1 - Introduction

The atomic beam machine at McMaster University is basically similar to other conventional atomic beam machines of the flop-in type. Since the days of Rabi (1938), these have consisted of the following essential components:

(i) High vacuum system;

(ii) A source of atoms;

(iii) A suitable collimating arrangement;

(iv) Deflection inhomogeneous magnetic fields;

(v) A variable homogeneous magnetic field;

(vi) A radio frequency field;

(vii) A detecting device.

Neutral atoms are thermally ejected from the slit (0.03 cm wide) in the source oven and enter a high vacuum chamber where, due to the low pressure (10^{-6} mm. of Hg) the mean free path is much larger than the length of the chamber. The beam of atoms,

while traversing its path from the oven to the detector, passes in succession through three magnetic fields. Two of them, called A and B, are inhomogeneous, while the third, C, is a variable homogeneous magnetic field. The A and B magnetic fields due to their inhomogenity can deflect atoms possessing magnetic moments, while the C field has no effect on their direction of travel.

A radio frequency magnetic field is superimposed on the C field and is capable of inducing transitions between the energy levels of the atom as it passes through that region. The frequency necessary to cause a transition is dependent upon the strength of the C field and upon the electric and nuclear properties of the atom. The A and B magnets and apertures act in such a way that they transmit only those atoms which undergo an appropriate transition in the C field region. The rest are thrown away. Typical beam trajectories are shown in Figure 3. By placing a suitable device at the exit slit of the machine one can detect the atoms which have undergone the transition. By measuring the strength of the C field and the frequency at which the transition occurs one can thus determine the various atomic and nuclear constants.

A detailed description of the machine has been given by Cameron (1962) and King (1960). In this chapter a very brief description is given and the various modifications and improvements made since then are mentioned.

FIGURE 3 TYPICAL ATOMIC BEAM TRAJECTORIES

A plan view of an atomic beam apparatus. Trajectories of two idealized atoms are drawn. In a flop-in apparatus, with the fields and gradients of the A and B deflecting magnets as shown, atoms arrive at the detector D only if the sign of the atomic moment changes sign in the region of homogeneous field C. Stop wire, which prevents the undeflected atoms to reach the detector, is represented by S.

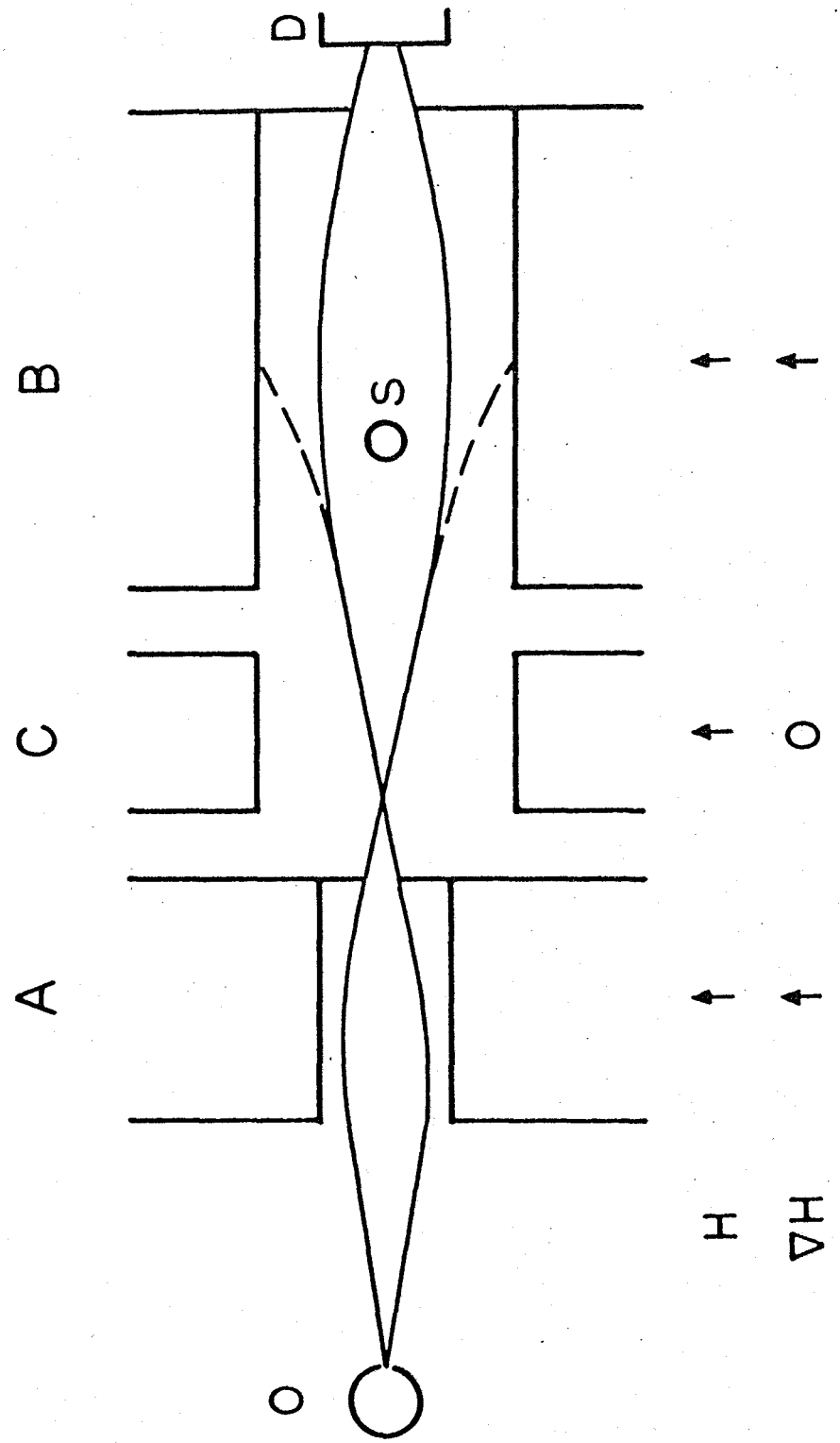
D
B
Os
C
O
A
H
ΔH
O

2 - Vacuum System

No modifications were made in the set up of the laboratory or the vacuum system as the existing facilities are considered to be quite adequate for the present experiment. With the two six inch, one four inch and one two inch diffusion pumps, all with liquid air traps and two mechanical rotary pumps, a vacuum of the order of 10^{-6} mm. of mercury can be obtained.

In order to maintain as low a pressure as possible over most of the beam path, inspite of the outgassing that occurs near the high temperature source, a series of baffles is provided and the isolation chamber is separately pumped. This design has the further advantage that most of the radioactive contamination is confined to the oven section.

3 - The Source Ovens

The source ovens (illustrated in Figure 4) are tantalum cylinders 5/8" in outside diameter and 1 inch high with screw lids and adjustable slits. The source is loaded in the oven by putting it in a carbon crucible which helps to prevent alloying of the source material with the tantalum. It is heated to the desired temperature by electron bombardment. The temperature may be measured using a Leeds and Northrup (Model 8622-C) optical pyrometer.

FIGURE 4 THE SOURCE OVEN

The drawing shows the parts of the source oven, the slits, the lid and the carbon crucible.

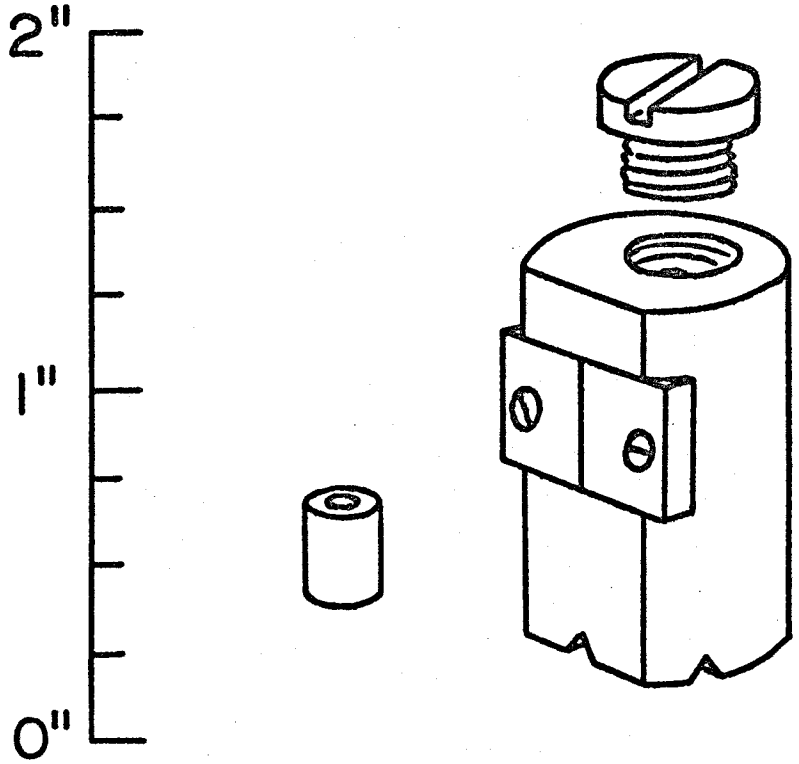
2"
1"
0"

The beam material used for calibrating the magnetic field of C magnet is loaded into an oven of stainless steel with approximately the same dimensions. Since the temperature involved is not so great, this oven is heated directly. For this purpose two holes are drilled near the bottom and tungsten heating coils are inserted in them.

Both the ovens are placed on an "oven bar" which can be introduced into the vacuum system via a two stage locking arrangement. The first stage reduces the pressure to 25 micron of Hg; after the second stage the pressure is about 5 microns and the bar can be inserted into the vacuum chamber. The entire process takes less than five minutes.

4 - The Magnet System

A sketch of the three electromagnets is shown in Figure 5 with the top of the case of the machine removed. The pole tips of the deflecting magnets A and B are sections of circular cylinders to provide a region of approximately uniform field gradient. A cross section of A-magnet pole pieces is shown in Figure 6. The B magnet has similar shape with the linear dimensions increased by a factor of two (15 inches in length) in order to subtend approximately the same angle at the source. The C magnet has plane parallel pole tips spaced 0.51 inches apart, to provide as uniform as possible a magnetic field.

FIGURE 5 THE MAGNET SYSTEM & GENERAL LAYOUT

A schematic view of the magnet system.

The prominant parts shown are:

1. A magnet
2. C magnet
3. B magnet
4. Oven interlock
5. Button interlock
6. Stop wire mechanism

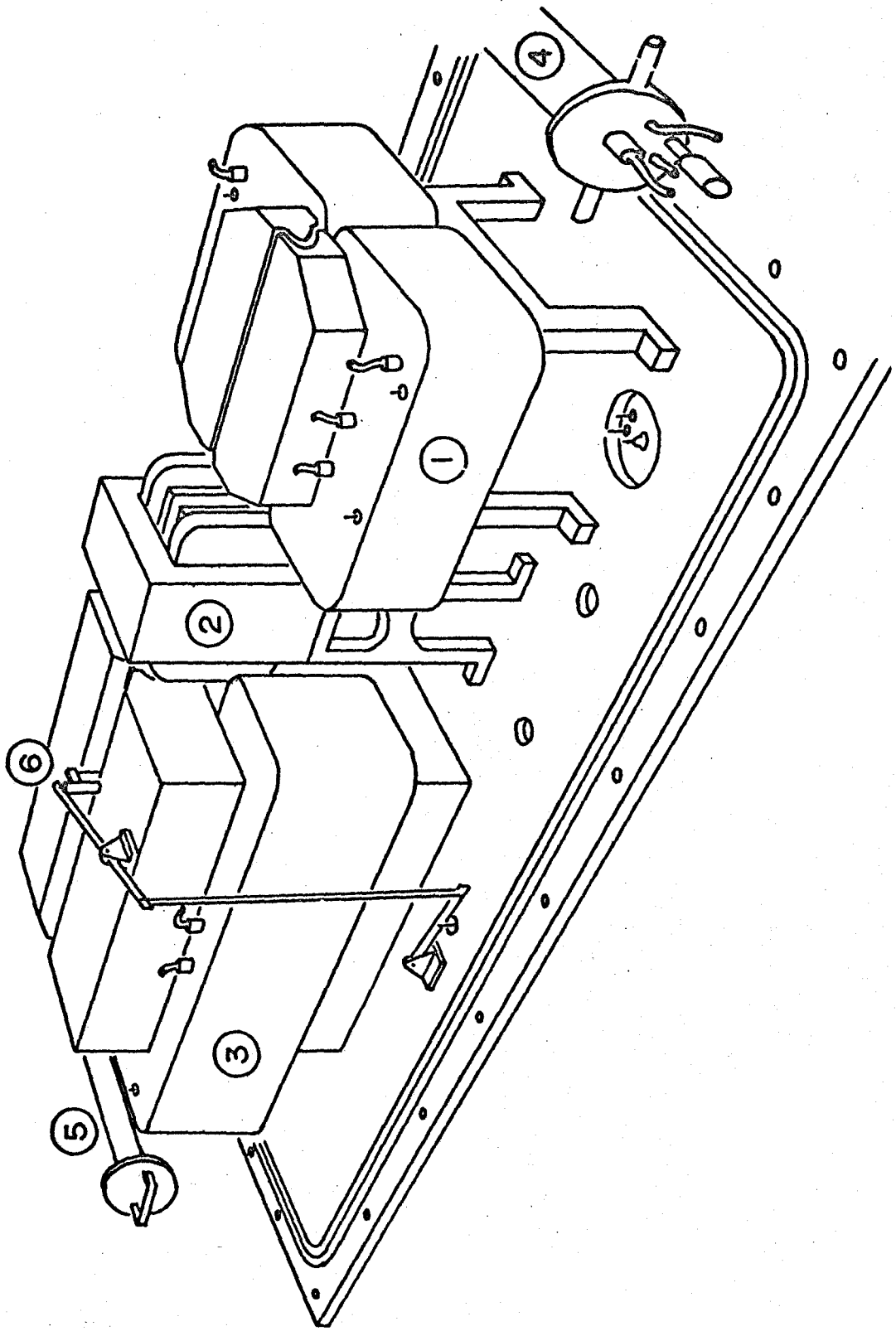
1
2
3
4
5
6

FIGURE 6 THE A-MAGNET POLE PIECES

The profile of the A magnet pole tips and the region through which the beam passes.

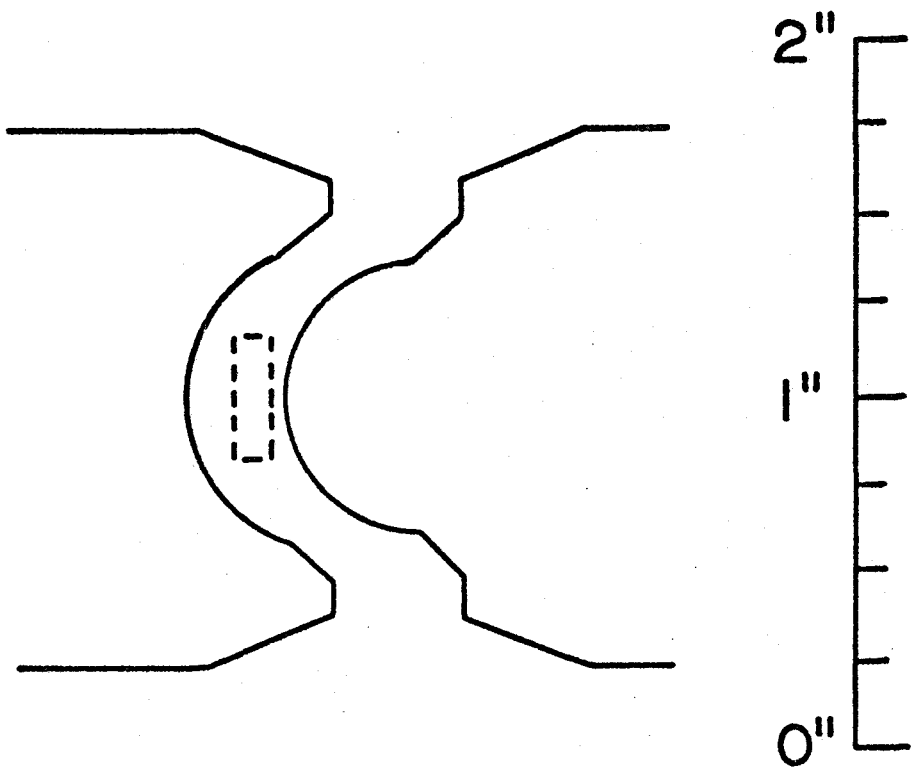
2"
1"
0"

5 - The Collimating System

The beam is collimated by two slits placed at the exi t end of each deflecting magnet. The one on the A magnet is adjustable in position to assist in initial beam alignment. The other can be changed in position and width. The most appropriate settings were ascertained before each radioactive run to get the maximum signal-to-noise ratio for both a Na^{23} beam and a stable indium beam.

In order to prevent the undeviated fast moving atoms from reaching the detector a stop wire is placed in the middle of the B magnet. This can be removed or inserted in the path of the beam with a lever arrangement at the bottom of the machine.

6 - Detecting Device

For detecting the sodium beam and the stable indium beam for initial alingment the surface ionization detector method was employed. (King, 1960, Cameron, 1962). In order to improve the efficiency of the detector wire the old detector wire was replaced by a new tungsten wire which was platinum-coated. This was done by evaporating the platinum in vacuum at a temperature of about 2800°C. The new platinum coated tungsten surface due presumably to its different work function, was found to be about five times more efficient than the old oxide-coated tungsten wire.

For the radioactive experiments, copper plated steel buttons were exposed in the beam for a known time. Their decay was then observed in low background β counters to determine the amount and half life of the activity deposited.

The Radiofrequency Equipment

The radiofrequency equipment consists of a signal generator a counter with appropriate transfer units for determing the frequency and arrangement for matching the load to the generator, and the loop for producing the required oscillating magnetic field. The oscillator used in the experiment (Wandel and Golterman LMS - 68) covers a frequency range from 0.35 to 960 Mc/sec. and is capable of delivering a power of up to 1 watt. The crystal controlled counter (Beckman Model 7170) has a stability of 1 part in 10^7 which was adequate. The loop used for the indium experiment is shown in the Figure 7. In consists of a shorted air dielectric coaxial line with a slot cut for the passage of the beam. The magnetic field produced by this loop circulates about the centre conductor with components both parallel and perpendicular to the C field. Thus it can be used for inducing both π and σ transitions.

In order to avoid a mismatch between the loop and the 50 ohm transmission line a tuning device is essential. This was provided by a double stub tuner and a trombone for changing the length of the line. The reflected wave was isolated with a directional coupler and applied to an oscilloscope. The complete arrangement is shown in Figure 8.

FIGURE 7 THE RADIOFREQUENCY LOOP

The radiofrequency loop used for this experiment. The beam passes through the slots and cut-away portion of the centre conductor.

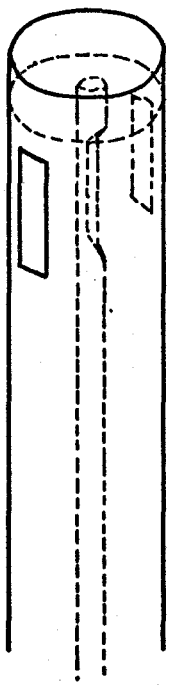

FIGURE 8 THE RADIOFREQUENCY EQUIPMENT

A block diagram of the radiofrequency equipment along with the tuning arrangement. The abbreviations in the various blocks stand for:-

SCOPE - Oscilloscope.

XTAL - Crystal detector manufactured by Telonic Company.

OSC - Oscillator (Wandelu, Goltermann, LMS 68).

TEE - TEE

ATTN - Attenuator 6db.

DC - Directional Coupler, M. C. Jones Corporation.

CNVTR - Converter (Beckman Amplifier, Model 7570).

DST - Double stub timer.

COUNTER - Beckman EPUT meter 7170.

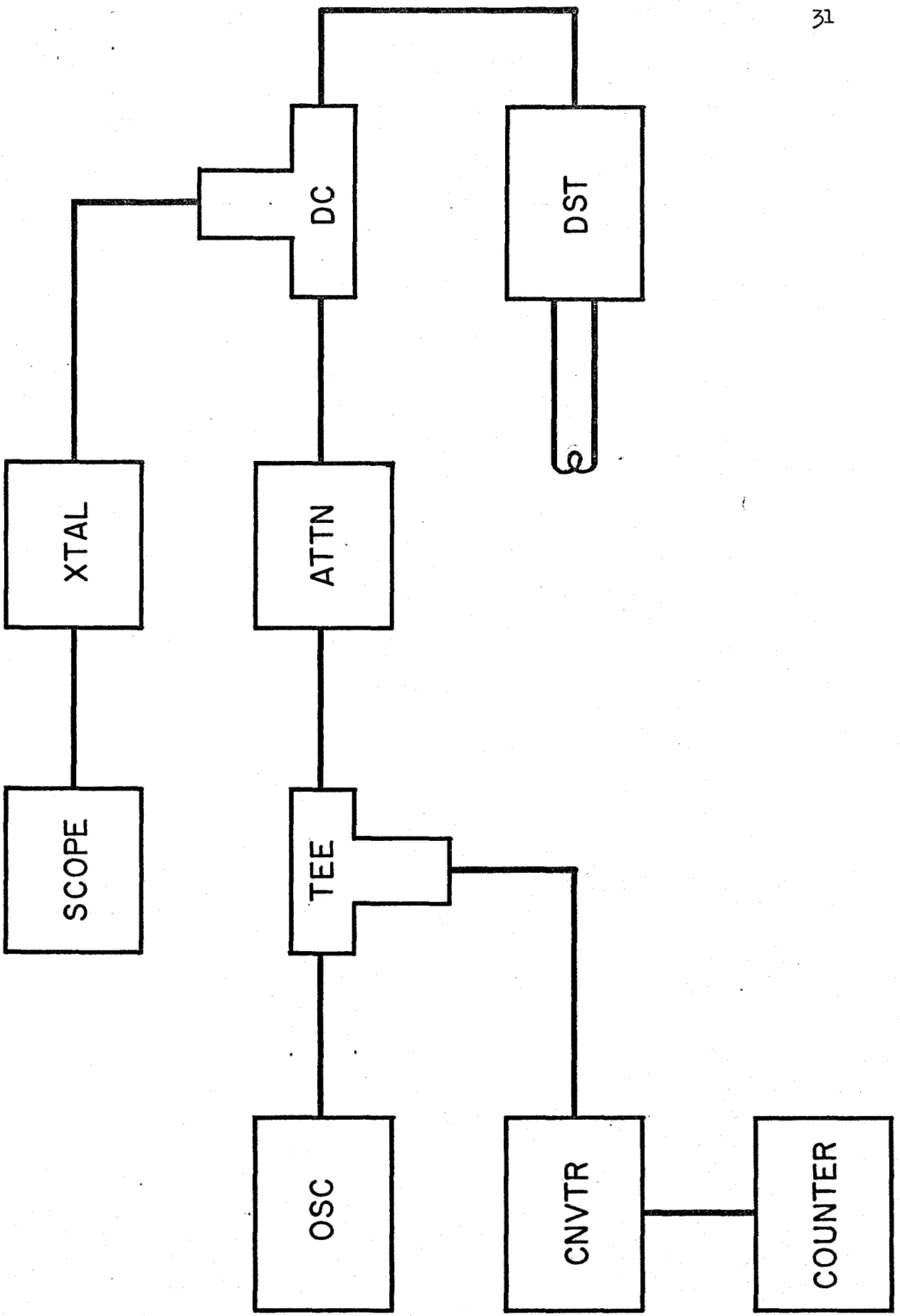
DC
DST
XTAL
ATTN
SCOPE
TEE
OSC
CNVTR
COUNTER

CHAPTER IV

EXPERIMENTAL METHOD

1 - The Indium Source Preparation

In^{117m} sources were prepared from natural cadmium by irradiating it in the thermal neutron flux of the McMaster reactor and allowing it to β decay. The reaction proceeds as follows

$$Cd^{116} \ (n,\gamma) \ Cd^{117} \xrightarrow{\beta^-} In^{117m} \xrightarrow{\gamma} In^{117}$$
$$\searrow^{\beta^-} \quad \swarrow^{\beta^-}$$
$$Sb^{117}$$

The specially rolled sheets of thickness .005 inches weighing two grams were shaped into hollow circular cylinders of approximate height 1.5" and diameter 0.65" to fit the reactor capsule without overlapping. This device is an attempt to minimize the problem of self shielding due to the very large cross section for neutron capture by Cd^{113}.

Unfortunately besides other isotopes, natural cadium contains Cd^{114} (28.86%) as well as Cd^{116} (7.58%) so that Cd^{115} and hence In^{115m} is produced in the irradiation too. The half-lives of In^{115m} and In^{117m}, 4.5 and 1.9 hours respectively,

are sufficiently the same that there is difficulty in extracting the amount of the latter present in a composite decay. Due to the different rates of growth of the two indium activities, a most suitable duration of inadiation can be found which will yield a suitable total activity and a good ratio of initial activities.

The calculations are based on the differential equations which govern the number of In^{117m} and In^{115m} atoms present at any time during irradiation and afterwards. If N_o denotes the number of parent cadmium atoms (Cd^{114} or Cd^{116}) in the sample, N, the number of Cd^{115} or Cd^{117} nuclei present at time t and N_2 the number of In^{115m} or In^{117m} nuclei, then

$$\frac{dN_1}{dt} = \sigma N_o \phi - \lambda_1 N_1$$

$$\frac{dN_2}{dt} = \lambda_1 N_1 - \lambda_2 N_2.$$

The cross-section for neutron capture is denoted by σ and ϕ is the neutron flux which is, of course, zero after the sample has been removed from the reactor. The half-lives of the radioactive cadmium and the induim are $.693/\lambda_1$, and $.693/\lambda_2$ respectively.

FIGURE 9 Production of In^{117m}

The graph shows the growth and decay of In^{117m} activity for different length of irradiation time. The vertical scale Y_1 is plotted in units of $\frac{3(\lambda_2 - \lambda_1)N}{N_o \phi \sigma}$ while Y_2 represents the Ratio of $\frac{In^{117m}}{In^{115m}}$ function. Curve (B) shows the In^{115m} activity. Curve (A) is to be read along the Y_2 scale.

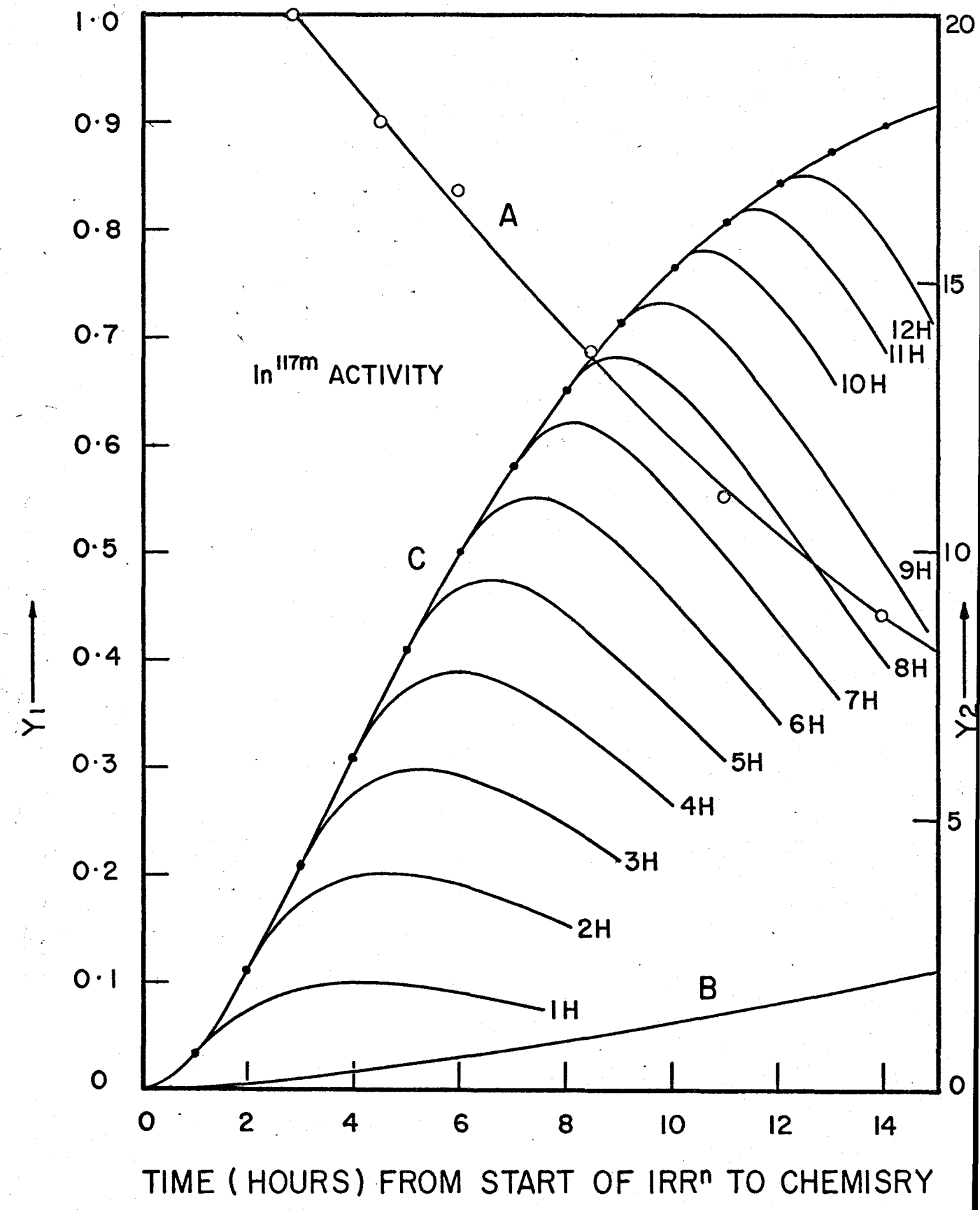
1·0
0·9
0·8
0·7
0·6
0·5
0·4
0·3
0·2
0·1
0
Y1
20
15
10
5
0
Y2
A
B
C
In^117m ACTIVITY
1H
2H
3H
4H
5H
6H
7H
8H
9H
10H
11H
12H
0
2
4
6
8
10
12
14
TIME (HOURS) FROM START OF IRRn TO CHEMISRY

Until the end of irradiation, t_R,

$$N_2 = \frac{N_o \sigma \phi}{\lambda_2} \left[1 - \frac{\lambda_2}{\lambda_2 - \lambda_1} e^{-\lambda_1 t} + \frac{\lambda_1}{\lambda_2 - \lambda_1} e^{-\lambda_2 t} \right] \quad t \leq t_R$$

After that, but before the isolation of the indium from its present cadmium

$$N_2 = \frac{N_o \sigma \phi}{\lambda_2 - \lambda_1} \left[(1 - e^{-\lambda_1 t_R}) \; e^{-\lambda_1 (t - t_R)} - \frac{\lambda_1}{\lambda_2} (1 - e^{-\lambda_2 t_R}) \; e^{-\lambda_2 (t - t_R)} \right]$$

$$t \gg t_R \; .$$

A graph showing these results is given in Figure 9. Also shown is the ratio of the activity of In^{117m} to that of In^{115m}. The half-lives and cross-sections were taken from the Nuclear Data sheets. It is noteworthy that the half-life of Cd^{117} is now reported to be three hours (Sharma, 1964) instead of fifty minutes, which is the value that caused Cameron to use a relatively short irradiation. For these experiments the irradiation time was chosen to be fourteen hours.

2 - Chemistry

After the irradiation the sample was transferred to a glove box in the radioisotope laboratory adjoining the atomic beam

apparatus. The basic principle of the chemistry was the same as described by Cameron (1962) except that, in view of the short half life of In^{117m}, every step was improved and thoroughly mastered in order to spend less time in chemistry. Typically, the time of receiving the sample from the reactor to the time of putting it in the machine was about 40 minutes.

Instead of dissolving the irradiated cadmium sample in about 4 mℓ. of concentrated HNO_3 it was dossolved in 8 mℓ. of concentrated HNO_3 already containing 25 mgms of stable indium to be used as carrier. In this way the time of dissolving the cadmium was curtailed to 8 or 10 minutes. With the addition of NH_4OH both cadmium and indium hydroxides precipitate. In an excess of ammonia, cadmium forms the soluble ammonium complex $Cd(NH_3)_4\ (OH)_2$ while indium hydroxide remains insoluble. The latter was separated by contrifuging the solution for two to three minutes. The collected residue of indium hydroxide was dissolved in a few drops of concentrated Hcℓ. In order to recover indium metal out of this solution about 75 mgms of aluminum filings were added to the weak solution. In about two minutes a black spongy mass formed near the surface of the liquid and could be easily picked up with a small glass shovel. The process was repeated in order to be certain that no indium remained in the solution. The collected spongy form of indium was rinsed with alcohol

and then compressed in a tube to squeeze out the remaining traces of water. After ensuring its dryness the tiny pill of sample was loaded in the oven which was then transferred to atomic beam machine.

In order to get a rough idea of the quantity of the precipitated indium the test tube containing the solution was brought near a survey-meter before and after recovery of the indium. The two readings always showed that less than 10% of the indium remained in the solution. It was in the best interest of the experiment not to waste time trying to retrieve the last small fraction.

3 - The Approach to the Experiment

The experiment is a difficult one because of the relatively short half-life of the isotope under study. This is aggravated by the necessity of a time-consuming chemistry and, particularly, by the curtailment of the useful counting time as the total activity of the source becomes more and more dominated by the In^{115m} which is unavoidably present. Thus it is important to expose the detector buttons at the desired frequencies as quickly as possible, so that counting may begin.

In addition, however, it is necessary to monitor the beam intensity which is particularly unstable at the beginning of a run

due to the appreciable increase in pressure in the oven chamber as outgassing occurs. In the customary technique, the beam is monitored between resonance exposures by interposing so-called "half-beam" buttons taken with the stop-wire removed from the beam path. This uses time that might otherwise have been used to improve the statistics of the resonance buttons. In a more recent technique, a simultaneous side-button monitor and resonance button are exposed. For an indium beam, which suffers only small deflections in the apparatus, this procedure seriously impairs the signal-to-background on the resonance.

The procedure adopted turns the disadvantageous presence of the In^{115m} into a useful tool. Off resonance it is still possible for some atoms to reach the detector. This residual beam, called the "r-f off", will reflect the isotopic composition of the beam and will be proportional to its intensity. Therefore, at a frequency off resonance for both In^{115m} and In^{117m}, a resonance button will receive activity of each kind in a ratio determined by the irradiation particulars for the source. At a resonant frequency for In^{115m} the ratio of In^{117m} to In^{115m} will diminish from that value and at a resonant frequency for In^{117m} the ratio will increase. Moreover, these ratios will be completely independent of the beam intensity. Of course, if the beam falls

to a very low value, both activities will approach zero and the statistical error on the ratio will be large. If the experimental data are taken in this way then there is no need for a beam monitor at all.

There is a further advantage to this approach. Since the hyperfine transitions in In^{115m} occur at frequencies known from the results of Cameron, it is possible to look for these and hence determine their resonance widths and depths. The frequencies of the corresponding In^{117m} resonances being sought are only a little different (but far outside the line-width) so it is reasonable to expect the r.f. power from the oscillator to be about the same. Thus, the resonance widths should be the same in the two cases. If the sources used in these tests are irradiated for the same time as those for the In^{117m} investigation, the In^{117m} : In^{115m} ratio on resonance should decrease by the same factor as that by which it will increase at the appropriate In^{117m} frequency. This means that the shape (width and height) of the resonances being sought can be known in advance. This is clearly an invaluable aid if the counting statistics are marginally poor.

On the basis of his measurements of the $\Delta F = 0$ transition in the $^2P_{1/2}$ state Cameron concluded that the value of $|a_{1/2}|$ for In^{117m} is 931.5 ± 2.0 Mc/sec. The frequency of the $\Delta F = \pm 1$, $(m = 0 \leftrightarrow m = 0)$ transition in the $^2P_{1/2}$ state of In^{117m} is therefore

expected to be 931.5 ± 2.0 Mc/sec with a very slight field dependent correction. When one considers that a single source lasts long enough to allow only some half dozen points which must be spaced, say, 50 kc/sec apart in order not to miss the resonance, it is clear that the scanning of a 4 Mc/sec search range would be a tedious task requiring at least 15 sources.

An alternative method is available, however. The ratio $a_{3/2}/a_{1/2}$ has been accurately measured for In^{113}, In^{115} and In^{115m} and the values found are 0.106096 ± 0.000039, 0.106124 ± 0.000001 and 0.106124 ± 0.000001 respectively. Thus it is verified to considerable precision that the ratio is isotope independent. If one assumes that the same ratio applies to In^{117m} the value of $|a_{1/2}|$ above requires that $|a_{3/2}| = 98.97 \pm 0.22$ Mc/sec. Hence, the frequency of the field independent hyperfine transition in the $^2P_{3/2}$ state of In^{117m} is expected to occur at 197.95 ± 0.45 Mc/sec. The search range is nearly five times smaller than that for the $^2P_{1/2}$ transition.

Unfortunately the resonance in the $^2P_{3/2}$ state will be of much less intensity. The fine structure separation, ΔE, between the $^2P_{1/2}$ ground state of indium and the $^2P_{3/2}$ metastable state is 2212 cm^{-1}. The temperature of the source is about 1150°C and this cannot be increased without greatly changing the rate of effusion from the oven thus impairing the vacuum in the apparatus.

Therefore, the relative population between these two states is 0.22 as given by

$$\frac{N(^2P_{3/2})}{N(^2P_{1/2})} = \frac{2(\frac{3}{2})+1}{2(\frac{1}{2})+1} \exp\left(-\frac{\Delta E}{kT}\right) .$$

this means that a resonance in the $^2P_{3/2}$ state will show only 1/10 the intensity of that in the $^2P_{1/2}$ state.

It was decided that, if the $^2P_{3/2}$ resonance can be seen by the ratio method in In^{115m} at its known frequency, then the narrower search range of the same transition in In^{117m} should be scanned first. If an indication of the latter is obtained then the correspondingly reduced frequency range in the vicinity of 931.5 Mc/sec can be examined to obtain better statistics and a reduced frequency error. On the other hand, if no indication of the $^2P_{3/2}$ resonance can be found either in In^{117m} or In^{115m} there is no alternative but to undertake a search over the full 4 Mc/sec range around 931.5 Mc/sec.

Finally, it should be noted that a small amount of enriched $Cd^{116}O$ is available, left over from the experiment to determine the spin of In^{117} (Cameron and Summers-Gill, 1962). The amount and its value precludes its immediate use in the search for the In^{117m} hyperfine transtions. If, however, the

experimental approach just described is successful then it should be possible to verify the frequencies with good statistics by using this material. Both because of the increased abundance of Cd^{116} and because of the absence of Cd^{113}, the counting rates should be high in spite of the fact that a 2 gram source is out of the question.

4 - Experimental Procedure

About five hours before each indium sample run the C field was calibrated by examing the Na^{23} Zeeman resonance. The frequency at which that occurs is directly related to the field since all the constants in the appropriate Hamiltonian are known to high precision. Two more checks of the same kind were done to verify the field stability - one just before the start of the chemistry and another just after the finish of the run. The field drift was usually quite small. In any case, at the low fields used, the σ-transitions in indium are field independent so that a precise value of H was unnecessary.

It was found that 25 mgm of indium carrier provides a beam lasting for about 55 minutes at 1150°C. This temperature is considered to be the most appropriate for beam production. Accordingly, the buttons were exposed in such a manner that the

overall time of exposure of six buttons was just less than the duration of the beam. The first two buttons were exposed for six minutes, the next two for seven minutes and the last two according to the time remaining to utilize all the beam.

The exposed buttons were put in a battery of six low background Geiger counters with anti-coincidence guard tubes. A record of the decay of each button was kept for about 20 hours after the run. In order to obtain sufficient points with minimum statistical errors the readings on the counters were taken at half hour intervals during the initial five or six hours. Thereafter, the interval between readings was increased proportionately as the time passed, reaching about 70 minutes at the end of the counting period. A typical graph of the decay of a button is shown in Figure 10. In order that the background counting rates might contribute minimum error, these were determined for a period of six to eight hours prior to the start of the run. The buttons subsequently to be used were placed in the counters so that any residual long-lived activity would be corrected for.

The composite decay curve of each button was separately resolved into two components of half lives 1.9 hours (In^{117m}) and 4.5 hours (In^{115m}) and extrapolated to the time of the end of the reactor irradiation. As the method adopted is different from

FIGURE 10 EXPERIMENTAL DECAY CURVE

A typical decay graph of a button is reproduced. The number of counts after subtracting the counter back ground are plotted on a logarithmic scale against time in hours on the linear scale.

(a) In^{117m}

(b) In^{115m}

(c) Composite Curve.

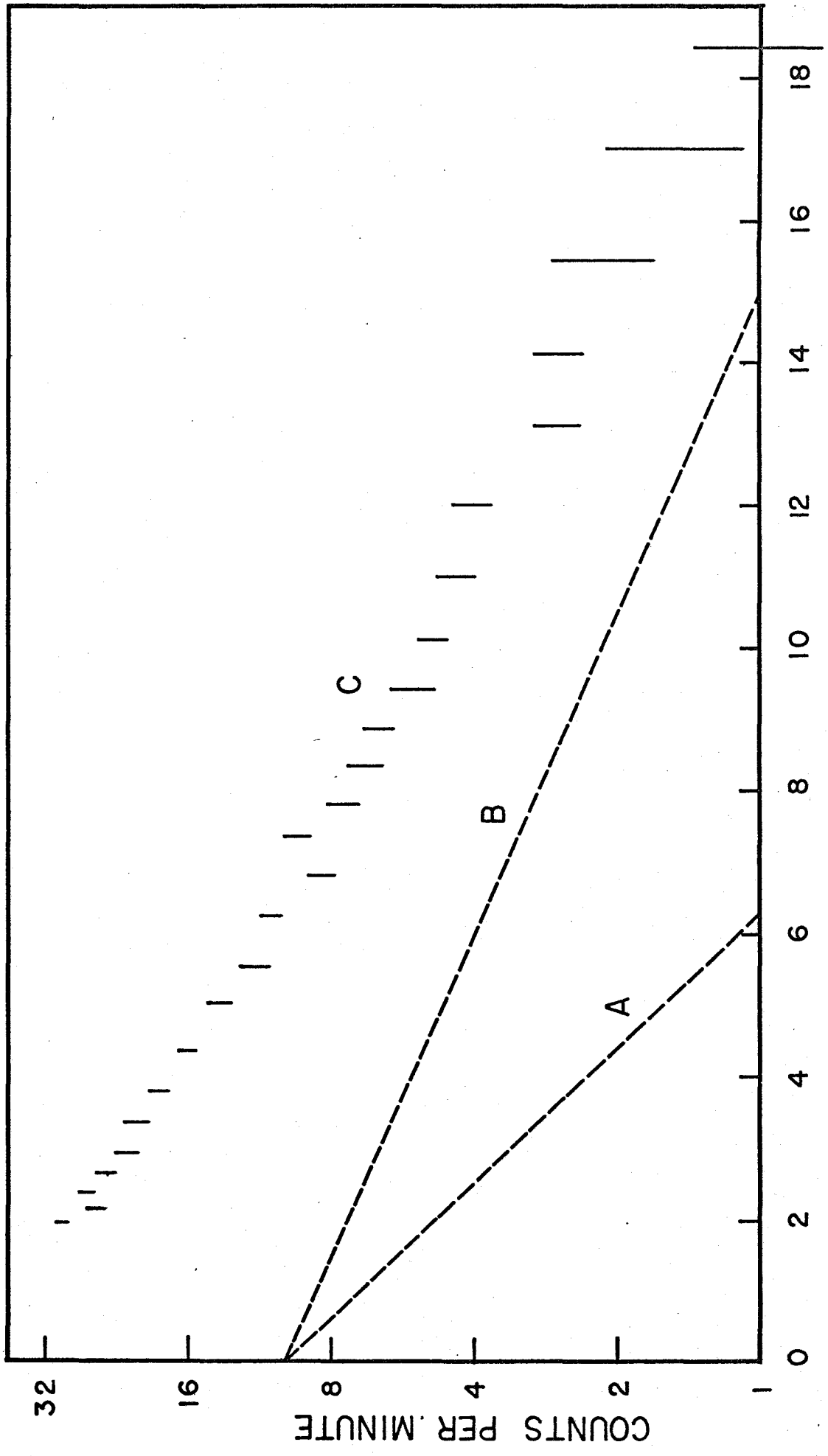
COUNTS PER MINUTE
32
16
8
4
2
1
0
2
4
6
8
10
12
14
16
18
TIME (HOURS)
A
B
C

the commonly used method of extrapolating the long-lived component and then subtracting that from the total counts, it will be of some interest to mention it here. The approach reduces the uncertainty when there is a relatively small difference in the half lives of the components.

A theoretical composite curve was drawn by assuming some initial ratio of In^{117m} and In^{115m} activities. In Figure 11 is shown a typical theoretical curve assuming the aforesaid ratio to be 2 : 1. The instantaneous ratio of activities takes on all values from 2 : 1 to 0 : 1 as one proceeds across the graph. The decay data of each button, plotted to the same scale on a second semi-logarithmic graph, were superimposed in turn on the master graph with the aid of a light box. Movement both vertically and horizontally is permitted, but the axes of the two graphs must remain parallel. When the most probable fit between the data and the master curve was obtained, the ratio of In^{117m} to In^{115m} at the time corresponding to the end of irradiation was noted from the master graph. The process was repeated three times for each button. Considering these three determinations, the mean value and the fitting error were decided. The results of such an analysis are included in Figure 10.

To obtain the results of a run it was then only a matter of plotting the ratios, either In^{117m} : In^{115m} or its reciprocal,

FIGURE 11 THEORETICAL COMPOSITE CURVE

A theoretical composite decay curve for In^{117m} and In^{115m} by assuming their initial ratio as 2 : 1 and then half lives 1.9 hour and 4.5 hours respectively. The various curves are:-

(A) In^{117m}

(B) In^{115m}

(C) Composite Curve

The scales are explained in Figure 10.

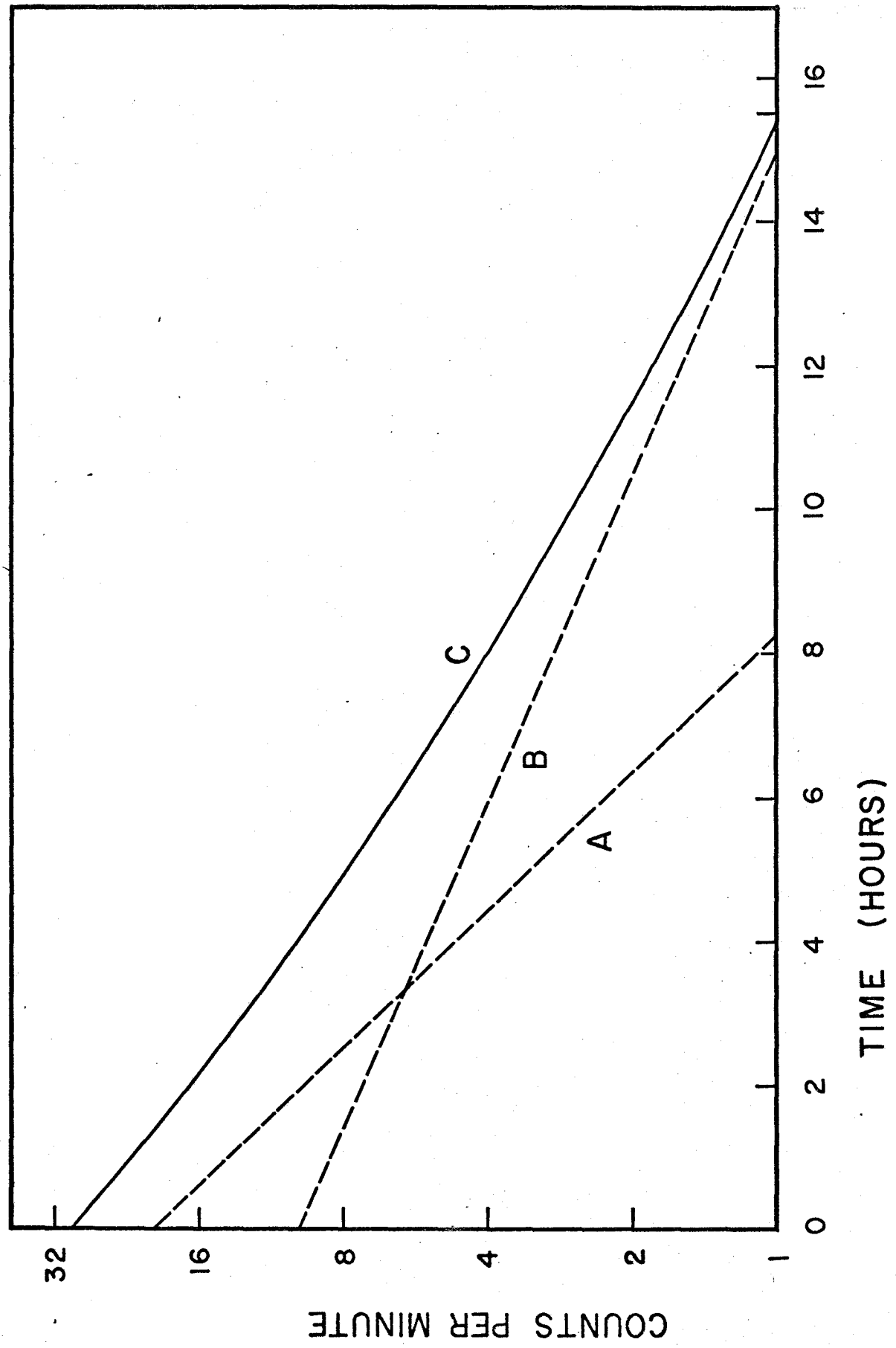
COUNTS PER MINUTE
32
16
8
4
2
1
TIME (HOURS)
0
2
4
6
8
10
12
14
16
A
B
C

versus the frequencies at which the buttons were exposed. In principle, the results of different runs can be combined, but it was convenient to differentiate the points for each source by using characteristic labels. Examples of such plots will be discussed in the next chapter.

CHAPTER V

RESULTS AND CONCLUSIONS

During the early stages of this work, while the chemistry was being optimized and the characteristics of the apparatus were being understood, many resonances in In^{115m} were examined using the high activity (~100 milliurie) sources that can be prepared in a 3- or 4-day inadiation. With such strong sources and with a pure activity (because of the long half life of Cd^{115} one can let the Cd^{117} and In^{117m} decay before even doing the chemistry) it is easy to obtain very good statistics. The field-independent σ-transitions in the $^2P_{1/2}$ and $^2P_{3/2}$ states are shown in Figures 12 and 13 respectively. For these data, the beam intensity was monitored by the usual "half-beam" method. The results,

$$|a_{1/2}| = 904.325 \pm 0.015 \text{ Mc/sec}$$

and

$$|a_{3/2}| = 95.962 \pm 0.008 \text{ Mc/sec},$$

are in excellent agreement with those of Cameron who quotes

FIGURE 12

A resonance curve corresponding to the $\Delta F = \pm 1$, $(m = 0 \longleftrightarrow m = 0)$ resonance in $^{2}P_{1/2}$ state of In^{115m}.

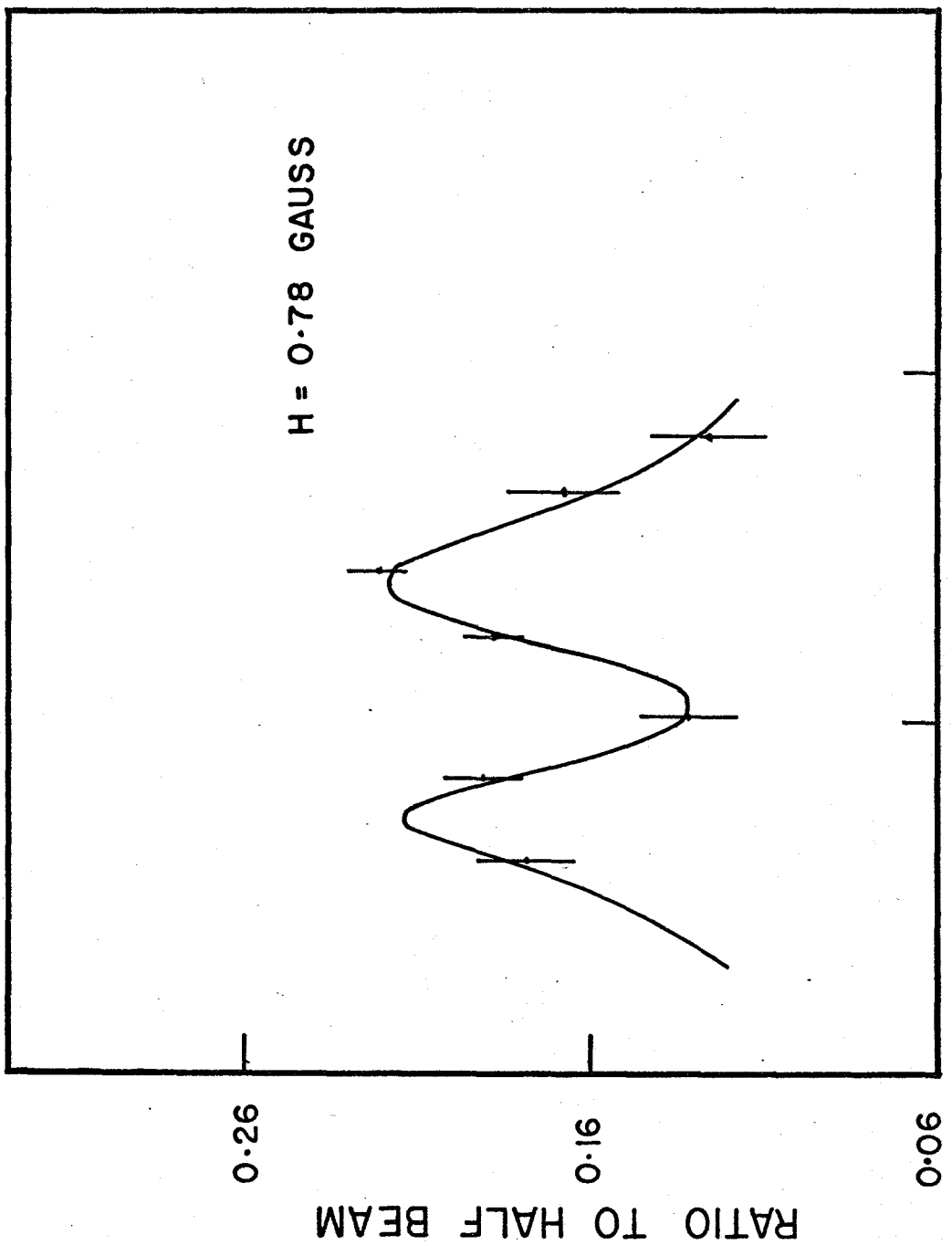
H = 0·78 GAUSS
RATIO TO HALF BEAM
0·26
0·16
0·06
904·17
904·32
904·47
FREQUENCY (MC/SEC)

FIGURE 13

A resonance curve corresponding to the $\Delta F = \pm 1$, $(m = 0 \longleftrightarrow m = 0)$ resonance in $^2P_{3/2}$ state of In^{115m}.

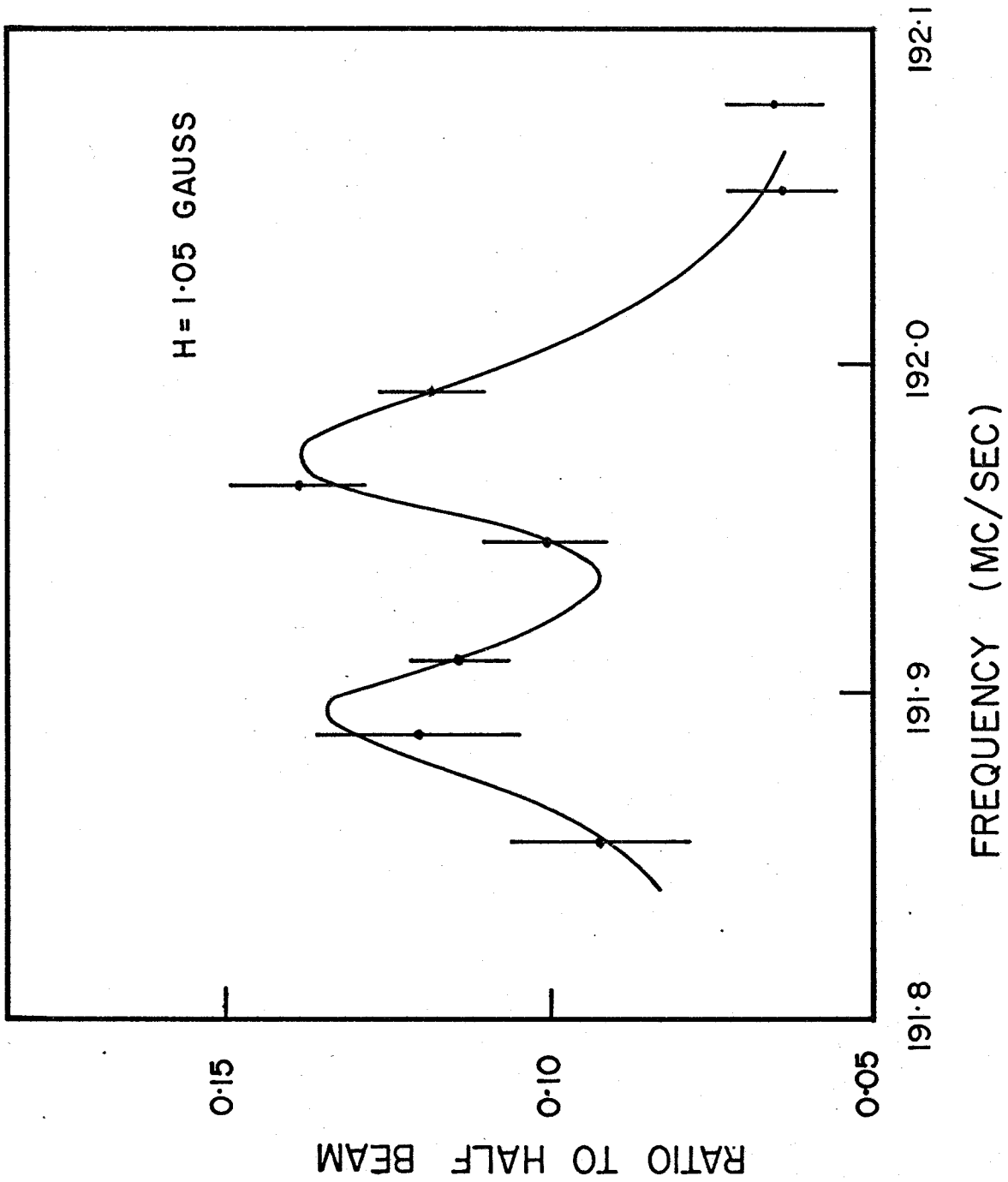

904.348 ± 0.016 and 95.973 ± 0.010 respectively. Since many parts of the apparatus have been altered in the interval between 1962 and the present this may be taken as strong evidence that no serious systematic error existed then or exists now. It is apparent that the resonance line widths in the present work are appreciably narrower than in the past. It is not known whether the improvement is due to better field stability, better field homogeneity or improved performance of the r.f. system.

As expected, the same resonances are much less definitive when obtained with a In^{115m} - In^{117m} source irradiated for 14 hours. These are shown in Figures 14 and 15, where the ratio of In^{115m} to In^{117m} activity is the ordinate. In neither case do the errors justify drawing a curve of the σ-resonance type. For the $^2P_{1/2}$ state, however, a resonance at 904.34 Mc/sec is a possible interpretation. The $^2P_{3/2}$ data show no sign of a dip in the ratio at 191.94, or of peaks in the vicinity of 191.89 and 191.98 Mc/sec. It is to be noted, however, that the reactor flux was not at its optimum for this irradiation.

In spite of the lack of success in seeing the $^3P_{3/2}$ resonance in In^{115m} the planned approach to the In^{117m} problem was followed through. Accordingly, a search for the analogous transition in In^{117m} was initiated over the frequency range 197.7

FIGURE 14

The results of the run made to find out the resonance frequency of In^{115m} $\Delta F = \pm 1, (m = 0 \leftrightarrow m = 0)$ in $^2P_{3/2}$ by using the ratio method. The big error bars do not permit the drawing of a σ resonance curve.

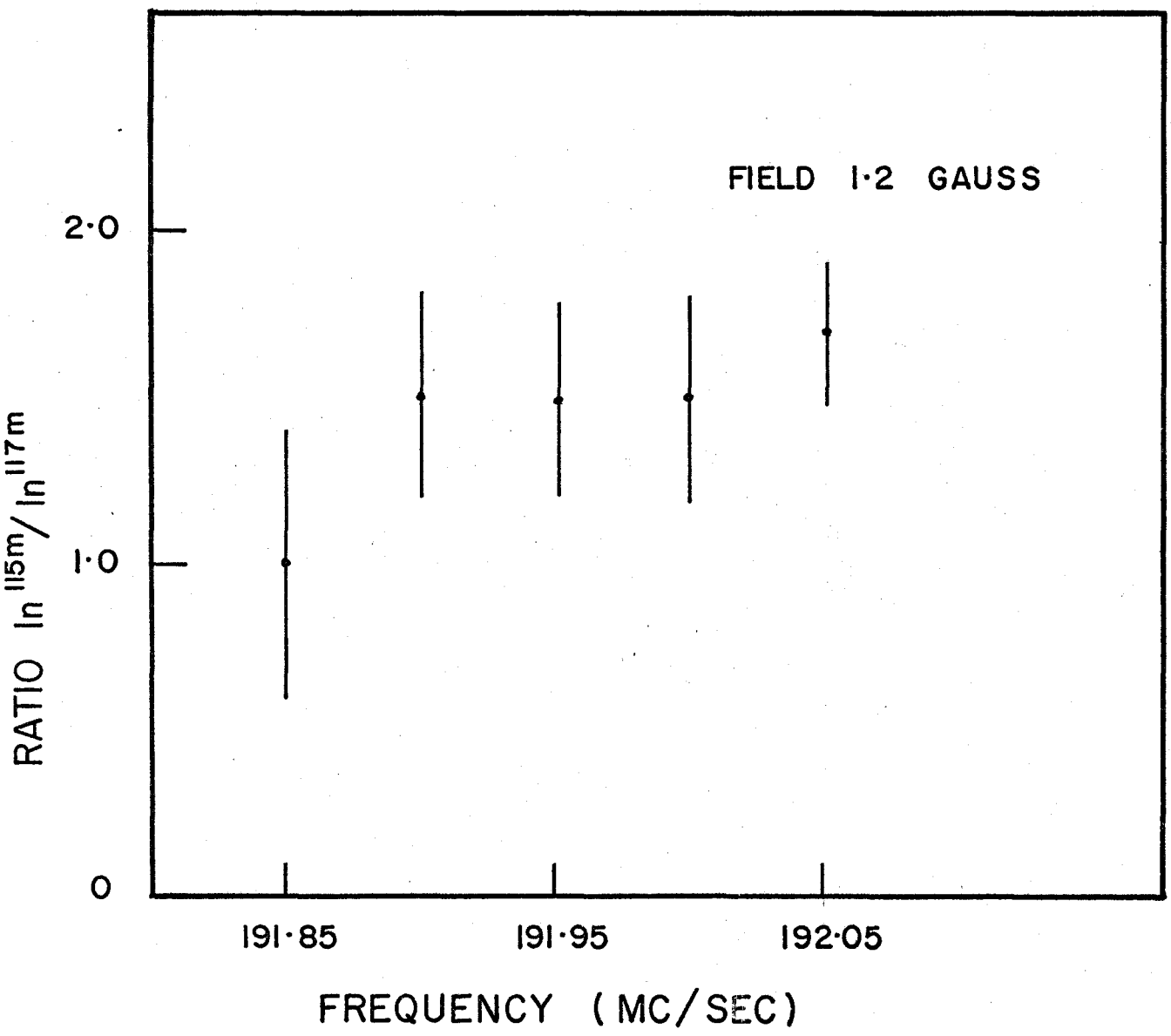
FIELD 1·2 GAUSS
2·0
1·0
0
RATIO In^{115m}/In^{117m}
191·85
191·95
192·05
FREQUENCY (MC/SEC)

FIGURE 15

The results of the run made for In^{115m} $\Delta F = \pm 1$ ($m = 0 \longleftrightarrow m = 0$) resonance in $^2P_{1/2}$ state by the ratio method.

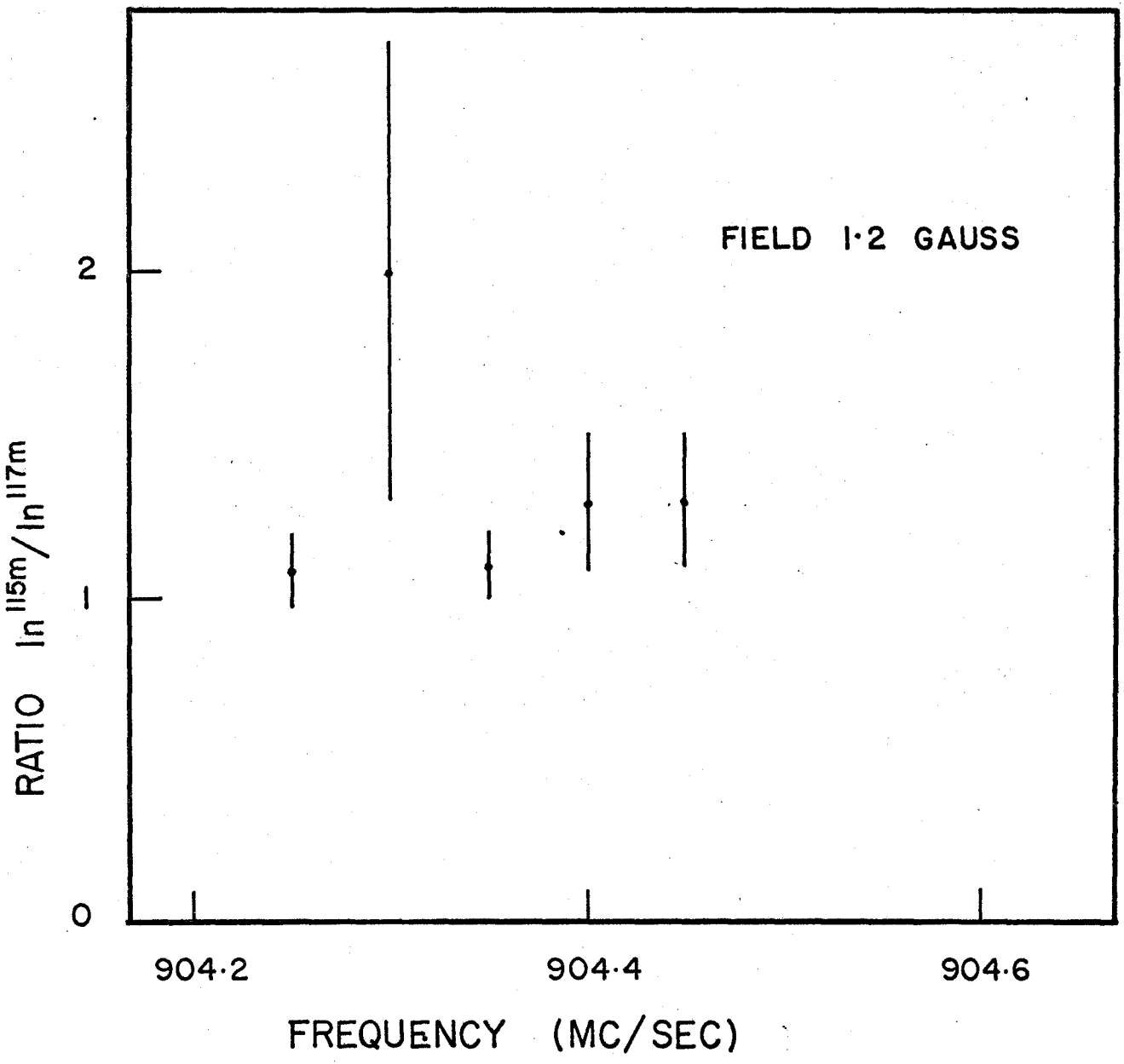
FIELD 1·2 GAUSS
RATIO In^{115m}/In^{117m}
2
1
0
904·2
904·4
904·6
FREQUENCY (MC/SEC)

to 198.2 Mc/sec. In the data of several runs there were indications of a σ-pattern centred at 198.02 ± 0.01 Mc/sec. A typical result is shown in Figure 16 which illustrates that the credibility depends crucially on the estimates of the uncertainties. Nevertheless, its repetition lends a certain confidence. Taking this frequency and applying the slight field correction appropriate to 1.09 gauss, one is led to the provisional value

$$\left| a_{3/2} \right| = 99.005 \pm 0.005 \text{ Mc/sec}$$

for In^{117m}.

If this value is correct and if the ratio of the coupling constants in the $^2P_{3/2}$ and $^2P_{1/2}$ states has a value close to 0.10612, the resonance in the $^2P_{1/2}$ state should occur at a frequency close to 933.0 Mc/sec. In three separate runs searching this region the ratio of In^{117m} to In^{115m} activities was significantly lower at 932.995 or 933.000 Mc/sec than on either side. Unfortunately, the details of the peaks are not quite the same, but this could be due to instrumental effects. The results of one such run are shown in Figure 17. In order to evaluate the reality of the counting errors, the frequency range from 932.7 to 932.9 Mc/sec was scanned on two occasions in 30 kc/sec steps. Compared to the region near

FIGURE 16.

The $\Delta F = \pm 1$ ($m = 0 \leftrightarrow m = 0$) resonance in $^3P_{3/2}$ state in In^{117m}.

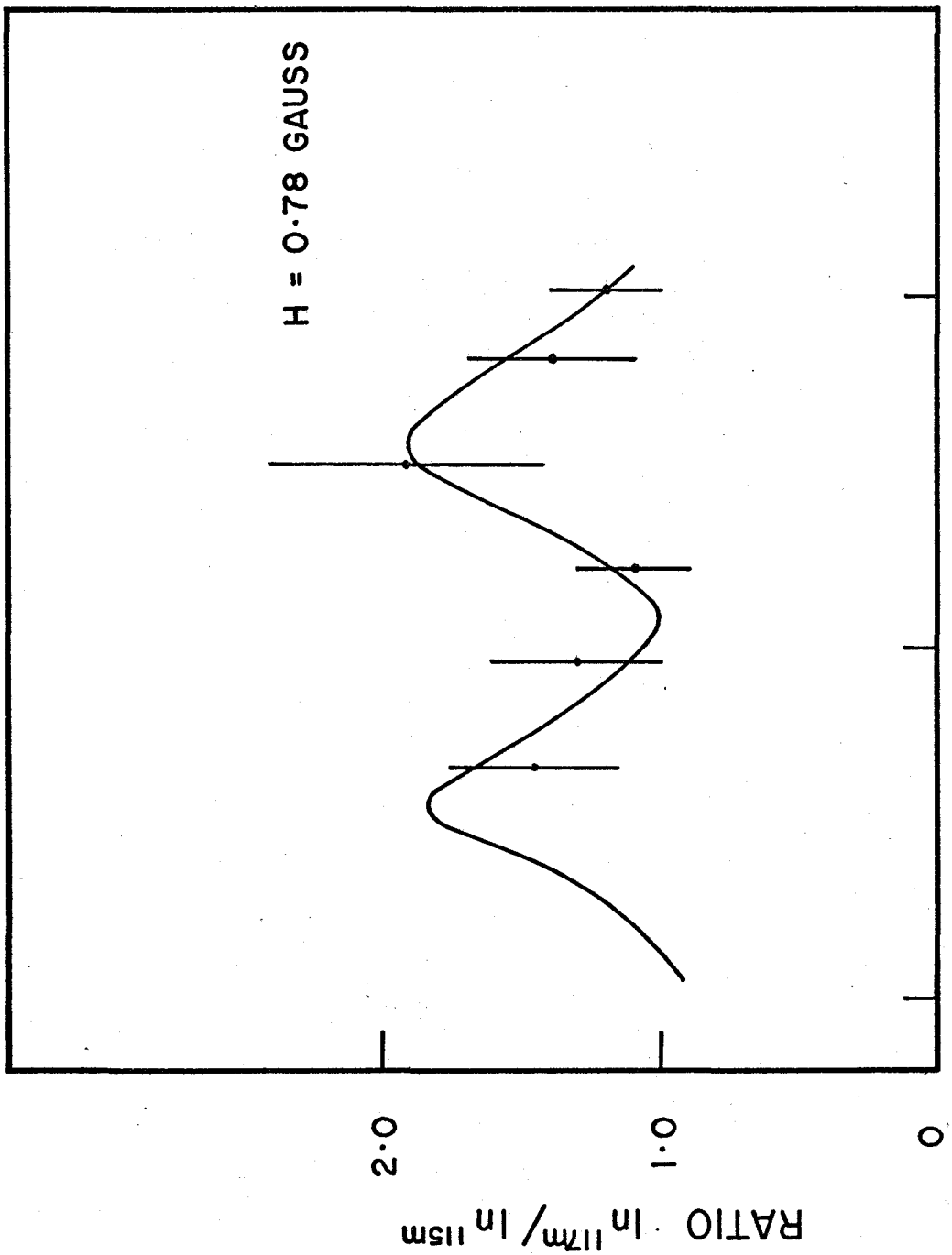
H = 0·78 GAUSS
RATIO · In^{117m}/In^{115m}
2·0
1·0
0
197·9
198·0
198·1
FREQUENCY (MC/SEC)

FIGURE 17

The $\Delta F = \pm 1$ ($m = 0 \leftrightarrow m = 0$) resonance in $^2P_{1/2}$ state of In^{117m}.

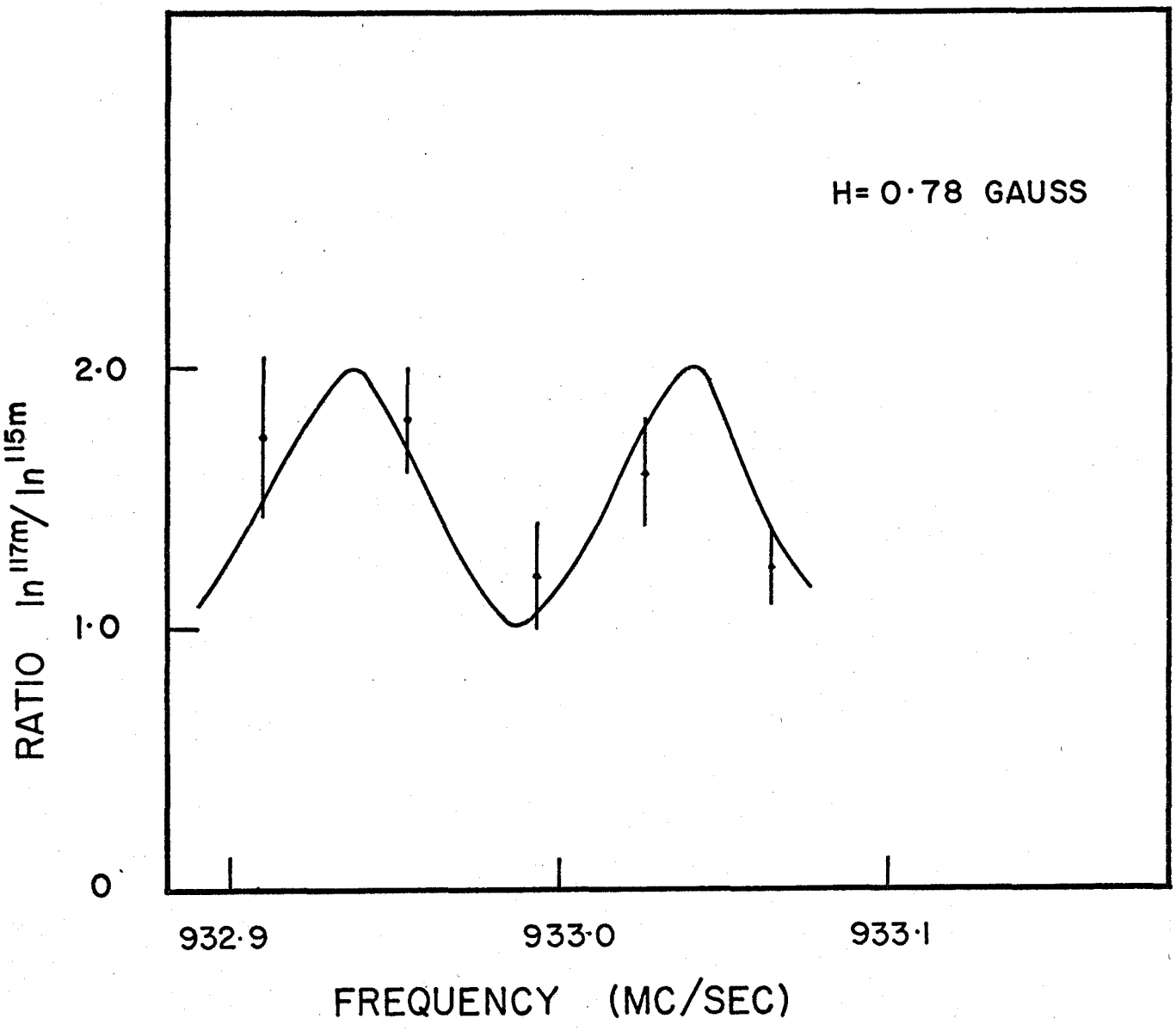
H= 0·78 GAUSS
2·0
1·0
0
RATIO In^{117m}/In^{115m}
932·9
933·0
933·1
FREQUENCY (MC/SEC)

933.0 Mc/sec the fluctuations in the activity ratio in this region were smaller and the errors are consistent with it being flat. Thus it seems quite probable that the $^2P_{1/2}$ has been observed. After field correction, the value of the coupling constant is given by

$$|a_{1/2}| = 932.996 \pm 0.012 \text{ Mc/sec.}$$

This value and that adopted provisionally for $a_{3/2}$ yield the ratio

$$\left|\frac{a_{3/2}}{a_{1/2}}\right| = 0.106115 \pm 0.000005,$$

not quite within the error of the very precise In^{115} result, but in fine agreement with the less precise values for In^{113} and In^{115m}. That such good agreement should be found, when there is no reason to expect constancy to a few parts per million from isotope to isotope, is a fact lending support to the view that both In^{117m} resonances have been detected.

Two further tests were planned. Unfortunately, only one has been possible, as the reactor has been either shut down or operating at scarcely one megawatt in the last several weeks.

One test would be to look for the $^2P_{1/2}$ fesonance at fields of 10 or 20 gauss. Such fields would shift the transition to higher frequency by 44 and 176 kc/sec respectively. If the dip in the activity ratio follows that prediction this would negate the possibility that the present observations are being caused by some unusual fluctuation in the r.f. signal delivered by the generator. The second test, as mentioned previously, involves using cadmium enriched in Cd^{116}. The results are shown in Figure 18.

The following remarks are made on the assumption that $^2P_{1/2}$ resonance, at least, has been detected in these experiments. From his observations of the $\Delta F = 0$ transition in the $^2P_{1/2}$ state of In^{117m}, Cameron was able to conclude that either $a_{1/2} = + 930.5 \pm 1.3$ Mc/sec or $- 932.7 \pm 1.3$ Mc/sec. Without any other data to assist in choosing between these alternatives, he had to adopt the negative value only provisionally based on the expectation from shell model considerations that the nuclear magnetic moment is negative. The value obtained in this work, $|a_{1/2}| = 932.996 \pm 0.012$ Mc/sec, is consistent with his negative result and quite inconsistent with the other. Thus one may conclude, from the two experiments combined, that

$$a_{1/2} = -932.996 \pm 0.012 \text{ Mc/sec.}$$

This implies, of course, that $a_{3/2}$ is also negative, but that conclusion adds nothing new.

FIGURE 18

The $\Delta F = \pm 1$ ($m = 0 \leftrightarrow m = 0$) resonance in $^{2}P_{1/2}$ state of In^{117m} using Enriched CdO.

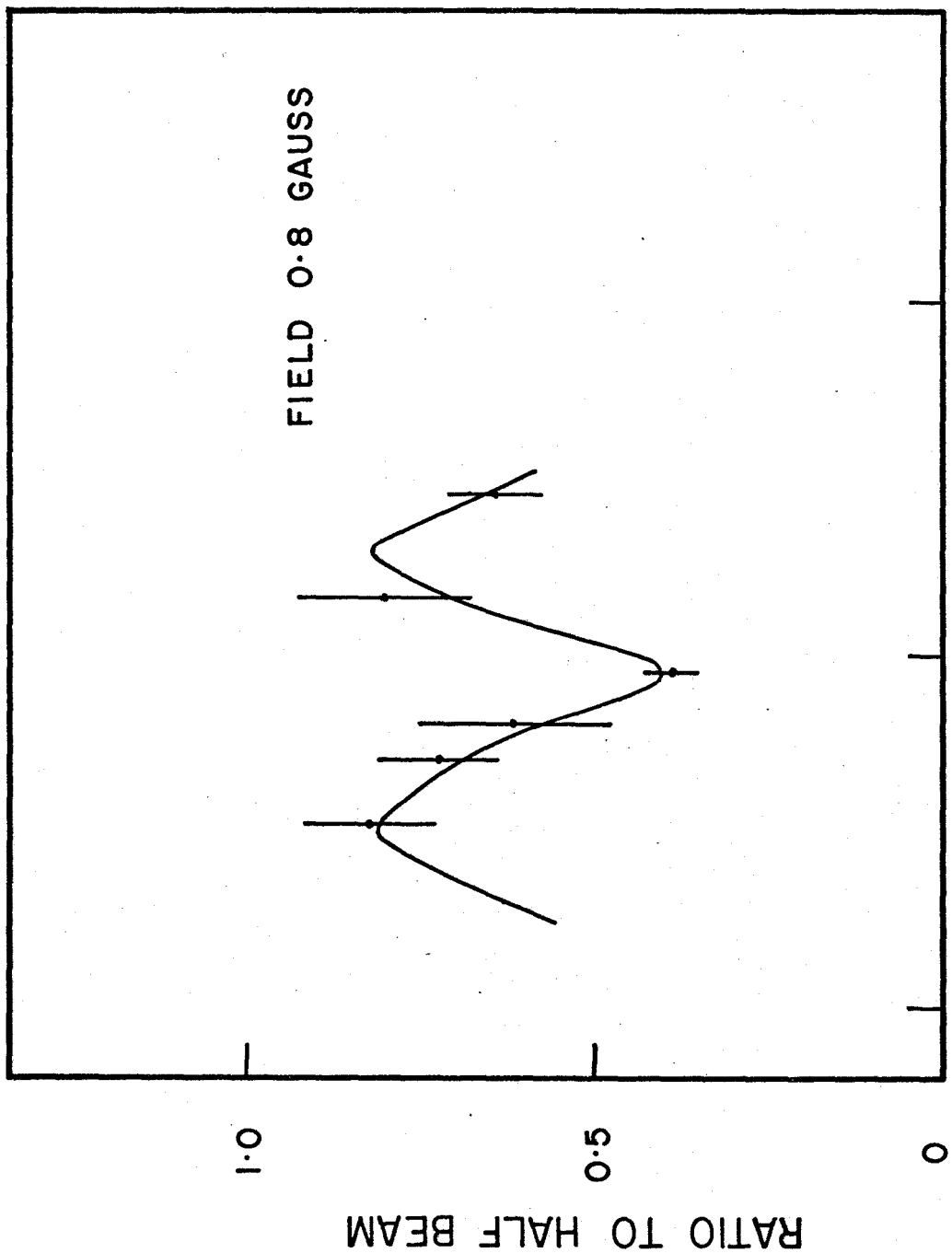
FIELD 0·8 GAUSS
RATIO TO HALF BEAM
1·0
0·5
0
932·9
933·0
933·1
FREQUENCY (MC/SEC)

Based on the foregoing value of $a_{1/2}$, one can calculate the nuclear magnetic moment of In^{117m} from the Fermi-Segrè formula. For a comparison isotope In^{115} ($a_{1/2}$ = 2281.910 ± 0.020 Mc/sec, μ_I = 5.5351 nuclear magnetons corrected for diamagnetic shielding, I = 9/2) may be used. The result for the corrected magnetic moment of In^{117m} is

$$\mu_I = -0.25146 \pm 0.00003 \text{ nuclear magnetons.}$$

This is to be compared with the value -0.24375 ± 0.00003 nuclear magnetons for In^{115m} which Lindgren (1964) obtained upon adjusting Cameron's result to the presently accepted magnetic moment of In^{115} quoted above. When one recalls that the Schmidt value for a $p_{1/2}$ proton is -0.264, the nearness of both these results to the value is rather interesting.

BIBLIOGRAPHY

Arima, A and Horie, H., 1954, Progr. Theoret. Physics (Japan) 11, 509.

Baker, F. S. and Brink, G. O., 1962, University of California. Lawrence Radiation Laboratory. Report UCRL 6772.

Bishop, C. T., 1962, Argonne National Laboratory Report ANL 6405.

Bohr, A. and Mottelson, B. R., 1953. Kgl. Danake Viderskab Selskab. Mat. -fys. Medd. 27, No.16.

Bornemeier, D. D. et al. Phys. Rev. 1964, B.740.

Breit, G. and Rabi, I. I. 1931. Phys. Rev. 38, 2082.

Breit, G. and Wills, W. A. Phys. Rev. 44. 470 (1933).

Cameron, J. A. Ph.D. Thesis, McMaster University (1962).

Cameron, J. A., King, H. J., Eastwood, H. K. and Summers-Gill, R. G. Canadian Journal of Physics, Vol. 40 (1962).

Childs, W. J. and Goodman, L. S. 1960. Phys. Rev. 118-1578.

Dunoyer, L. Dunoyer, Le Radium 8, p.142 (1911)

Fermi, E. and Segree, E. Z. Physik, 60 P.320 (1930).

Goodman, L. S. 1960, Rev. Sci. Instr. 31, 1351.

Goodman, L. S. and Wenlev, S. 1955. Phys. Rev. 1245.

Kellogg, J., Ramsey, N. Rabi, I. and Zacharias. Phys. Rev. 56, p.782 (1939).

King, H. J. 1960, Ph.D. Thesis, McMaster University.

King, H. J., Cameron, J. A., Eastwood, H.K. and Summers-Gill, R. G., 1961, Canadian Journal of Physics, 39, 230.

Kopperman, H. 1958. Nuclear Moments. (Academic Press, New York).

Kusch, P. and Hughes. "Atomic and Molecular Beam Spectroscopy", Encyclopedia of Physics. Springer-Verlag, Berlin, (1959), Vol. XXXXII/I.

Lindgren, I. 1964. Table of Nuclear Spin and Moments, Perturbed Angular Correlations, published by North-Holland Pub. Co., Amsterdam.

Marino, L. L., 1959. University of California. Lawrence Radiation Laboratory Report UCRL 8721.

Mayer, M. G. and Jensen, J. H. D. 1955. Elementary Theory of Nuclear Shell Structure.

Nilsson, S. G. 1955. Kgl. Danske Viderskab Selskab. Mat, -fys. Medd. 29, No.16.

Rabi, I. I. and Cohen, V. W. 1933, Phys. Rev. 43, 582.

Rabi, I. I., Zacharias, J. R., Millman, S. and Kusch, P. 1938, Phys. Rev. 53, 318.

Ramsey, N. F. 1956. Molecular Beams (Oxford University Press).

Ramsey, N. F. and Purcell, E. M. 1950, Phys. Rev. 78, 807.

Smith, J. H., Purcell, E. M. and Ramsey, N. F. Phys. Rev. 108, 120 (1951).

Smith, K. F. Molecular Beams.

Schmidt, T. 1937. Z. Physik 106, 358.

Schwartz, C. 1955. Phys. Rev. 97, 380.

Sharma, R. P. et al. Phys. Rev. 134, May 1964.

Sharma, R. P. et al. Tata Institute of Fundamental Research, Bombay, India. NP - 13020 pages 34-8. 1963.

Stern, O. 1921. Z. Physik, 7 249.

Woodgate, G. K. and Hellwarth, R. W. 1956, Proc. Phys. Soc. (London).

Zacharias, J. R. 1942. Phys. Rev. 61, 270.